UNIVERSITÉ DU QUÉBEC À MONTRÉAL

ÉVALUATION DE LA PERFORMANCE DU MODÈLE RÉGIONAL CANADIEN DU CLIMAT POUR SIMULER LES CYCLONES EXTRATROPICAUX AU NORD-EST AMÉRIQUE DU NORD

MÉMOIRE

PRÉSENTÉ

COMME EXIGENCE PARTIELLE

MAÎTRISE EN SCIENCES DE L'ATMOSPHÈRE

PAR

MAXINE CLOUTIER-GERVAIS

NOVEMBRE 2025

REMERCIEMENTS

Merci à Alejandro, grâce à qui je sors de ce projet en étant une jeune scientifique beaucoup plus expérimentée. Sa façon de diriger m'a permis de développer une autonomie exemplaire dans laquelle j'ai pu oser nourrir ma curiosité scientifique, car je savais qu'il n'était jamais trop loin pour me ramener sur le droit chemin si nécessaire.

Je remercie également mes codirecteurs Dominic et Philippe. L'attention aux détails et le côté très méthodique de Dominic m'ont permis de maîtriser mon projet comme le fond de ma poche, et les commentaires de Philippe ont toujours ouvert des discussions pour amener le projet plus loin et m'ont inspirée à créer des figures qui frôlent la perfection.

Un merci tout spécial à Katja qui m'a guidé (si ce n'est pas pour dire pris par la main) au tout début de mon projet pour manipuler des fichiers avec lesquels j'étais moins à l'aise, et à François pour avoir toujours été disponible pour m'aider côté programmation et informations techniques. Un énorme merci également à tous ceux au département qui ont contribué de proche ou de loin à la réalisation de ce projet.

J'ai grandement évolué en tant que personne pendant la réalisation de cette maîtrise, sur tellement de facettes. Félix peut en témoigner, car il a été à mes côtés autant lors des moments difficiles que lors des plus joyeux. Pour avoir été écoutant, tolérant et rassurant pendant ces moments, merci.

Lorsque j'avais besoin d'une petite pause pour retourner à ma ville natale et profiter d'un peu de zoothérapie (bonjour Goliath et Ana), mes parents m'ont toujours accueilli les bras ouverts et se sont assurés que je ne reparte jamais à Montréal sans un pot de sauce spaghetti. Je pourrais les remercier à l'infini pour tout ce qu'ils ont fait pour moi, mais je me contenterai ici de les remercier de m'avoir soutenue lors des deux dernières années.

Pour terminer, je remercie Bring Me the Horizon, mon groupe préféré depuis mon adolescence, qui ont sorti le 11 juillet 2025 un album de leurs chansons en version lo-fi. Pouvoir écouter leur musique pendant la rédaction de mon mémoire en tant qu'adulte a été à la fois motivant et nostalgique.

DÉDICACE

Pour Marie-Ève, qui m'accompagne toujours de là-haut : regarde ce qu'on a accompli.

TABLE DES MATIÈRES

TABLE DES FIGURES

LISTE DES TABLEAUX

ACRONYMES

CP	Cumulus Parameterization
CPRCM	Convection Permitting Regional Climate Model
CRCM6-GEM5	Sixth version of the Canadian Regional Climate Model
DJF	December-January-February
ERA5	Fifth version of the ECMWF Re-Analysis
ETC	Extratropical Cyclone
GCM	Global Climate Model
IMERG	Integrated Multi-satellitE Retrievals for Global precipitation measurement
ISD	Integrated Surface Database
ISD2ERA	Integrated Surface Database to ERA5
JJA	June-July-August
MAM	March-April-May
MSLP	Mean Sea Level Pressure
NA	North America
NENA	Northeastern North America
NEUS	Northeastern United States
P3	Predicted Particle Properties
MRC	Regional Climate Model
RCM12	CRCM6-GEM5 model at ~12-km horizontal grid spacing
RCM2.5	CRCM6-GEM5 model at ~2.5-km horizontal grid spacing
SON	September-October-November
VORT	850-hPa vorticity

LISTE DES SYMBOLES ET UNITÉS

PR	Taux de précipitation horaire
WS	Vitesse du vent soutenu près de la surface
$F_{ETC}^{\geq\theta}$	Champs de surface associé à un ETC qui dépasse un seuil θ. La variable F représente soit la somme des taux de précipitation horaires PR ou la somme des vitesses du vent près de la surface WS
$\hat{F}_{ETC}^{\geq\theta}$	Champs de surface normalisé associé à un ETC qui dépasse un seuil θ
$\Delta\hat{F}_{ETC}^{\geq\theta}$	Biais entre le champ de surface normalisé qui dépasse un seuil θ simulé et observé par un produit référentiel
p_{ETC}	Probabilité d'avoir un événement de cyclone extratropical à un endroit donné
$\mu_{F,ETC}^{\geq\theta}$	Intensité moyenne d'un champ de surface $F_{ETC}^{\geq\theta}$ pendant les événements de cyclones extratropicaux.
N_{tot}	Total du nombre d'heures disponibles dans un jeu de donnée
N_{ETC}	Nombre d'heures durant laquelle un endroit donné est dans un rayon de 1000 km d'un cyclone extratropical

RÉSUMÉ

La capacité des modèles régionaux du climat à convection explicite à simuler les cyclones extratropicaux (ETCs) ainsi que les vitesses de vent près de la surface et les précipitations associées demeure peu explorée. Cette étude présente la première évaluation de la sixième version du Modèle régional canadien du climat (MRCC6-GEM6) à cette fin sur le nord-est de l'Amérique du Nord. Deux configurations du modèle sont analysées : une grille de ~12 km pilotée par la réanalyse ERA5, et une version à ~2,5 km, imbriquée dans la simulation à 12 km. Les ETCs sont identifiés et suivis à l'aide d'un algorithme lagrangien de suivi des tempêtes, et leurs trajectoires, intensités et durées de vie sont évaluées en comparaison avec ERA5. Les vitesses de vent et les précipitations associées aux ETCs simulés sont comparées aux observations issues de stations in situ (ISD), de données satellitaires (IMERG) et radar (StageIV) sur une région commune du nord-est des États-Unis. La simulation à 12 km reproduit des trajectoires et durées de vie de cyclones comparables à celles d'ERA5, tandis que la version à 2,5 km génère un plus grand nombre de tempêtes, d'une durée plus longue. Les deux configurations reproduisent les principales caractéristiques des champs de surface associés aux ETCs, mais le modèle à 2,5 km représente mieux les taux de précipitation extrêmes et réduit les biais des vitesses de vent. La décomposition des biais des champs de surface indique que les écarts proviennent principalement de l'intensité des événements d'ETCs, et qu'une fréquence plus élevée de tempêtes ne se traduit pas nécessairement par des totaux de précipitation plus importants. Dans l'ensemble, les deux configurations reproduisent adéquatement les caractéristiques des ETCs, mais la version à convection explicite (2,5 km) s'avère mieux adaptée aux analyses climatiques à l'échelle locale.

Mots clés : Cyclone extratropical, modèle régional à convection explicite, précipitations horaires, vents près de la surface

INTRODUCTION

Les cyclones extratropicaux (ETCs) constituent un élément central dans la circulation atmosphérique globale et le transport d'humidité aux latitudes moyennes (Catto et al., 2019), apportant la majeure partie des précipitations annuelles dans l'hémisphère Nord (Hawcroft et al., 2012). Outre leur rôle fondamental dans la climatologie aux latitudes moyennes, ces systèmes synoptiques sont à l'origine d'événements extrêmes de vent et de précipitation (Booth et al., 2015; Chen & Di Luca, 2025; Pfahl & Wernli, 2012), causant des dommages importants aux infrastructures humaines et aux écosystèmes (Ashley & Black, 2008; Sibley, 2010).

Le nord-est de l'Amérique du Nord concentre une part importante de la population de cette région, avec plus de 65 % des Canadiens résidant à l'est du pays (Statistique Canada, 2025) et où se trouvent plusieurs des États américains les plus densément peuplés, tels que le district de Columbia, le New Jersey et le Rhode Island (United States Census Bureau, 2025). Cette forte présence humaine dans une région fréquemment touchée par les ETCs accentue la vulnérabilité aux aléas associés à ces systèmes. En effet, dans le nord-est de l'Amérique du Nord, plus de 60 % des épisodes de précipitations extrêmes survenus annuellement sont associés à ces systèmes (Chen & Di Luca, 2025; Pfahl & Wernli, 2012). Par ailleurs, Booth et al. (2015) ont démontré que plus de 80 % des épisodes hivernaux de vents forts le long de la côte est des États-Unis, définis par des vitesses dépassant le temps de retour de 1, 3 ou 5 ans à plusieurs stations, coïncident avec le passage d'un ETC. Un exemple marquant est la tempête d'Halloween de 2019 qui a frappé le nord-est de l'Amérique du Nord, causant plus de 250 millions de dollars canadiens en dommages assurés au Canada, avec des rafales dépassant 100 km/h le long de la côte est et des précipitations totales supérieures à 100 mm dans le sud du Québec (Insurance Bureau of Canada, 2019). Dans un contexte de changement climatique, les projections indiquent que les ETCs génèreront davantage de précipitations (Hawcroft et al., 2018; Zappa, Shaffrey, & Hodges, 2013), tandis que des modifications possibles des trajectoires de ces systèmes pourraient entraîner des variations significatives des vitesses des vents locaux (Li et al., 2014; Priestley & Catto, 2022; Seiler & Zwiers, 2016; Zappa, Shaffrey, Hodges, et al., 2013). Ces perspectives renforcent l'importance de produire des projections climatiques fiables concernant la fréquence et l'intensité des ETCs afin de mieux anticiper l'évolution des aléas engendrés par ces systèmes au cours des prochaines décennies.

L'intensité dynamique des ETCs est traditionnellement quantifiée à l'aide de métriques clés telles que le tourbillon, la pression moyenne au niveau de la mer ou les vents près de la surface, extraits à partir de produits de réanalyses ou de modèles climatiques (Seiler et al., 2018; Zappa, Shaffrey, & Hodges, 2013). Il existe un consensus largement partagé dans la littérature selon lequel la résolution horizontale relativement grossière des modèles de circulation générale (MCGs), tels que ceux du projet d'intercomparaison des modèles couplés (CMIP), conduit à une sous-estimation systématique de l'intensité des ETCs (Colle et al., 2013; Di Luca et al., 2016; Jiaxiang et al., 2020; Poan et al., 2018; Priestley et al., 2020; Seiler et al., 2018; Trzeciak et al., 2016; Zappa, Shaffrey, & Hodges, 2013). D'ailleurs, une analyse historique de Colle et al. (2015) portant sur l'activité des ETCs le long de la côte est des États-Unis a montré que les MCGs peinent à représenter certains processus dynamiques essentiels pour le développement et l'intensification des ETCs, tels que le gradient de température à la surface de la mer, le relâchement de chaleur latente et les interactions avec le courant-jet. De manière similaire, Poan et al. (2018) ont comparé les activités des ETCs simulés par deux MCGs de génération CMIP5 avec une résolution horizontale de 1.875° avec la réanalyse nord-américaine régionale (NARR). L'étude révèle que même si l'occurrence des ETCs simulée en Amérique du Nord est comparable à celle de la réanalyse, la faible résolution horizontale limite la représentation des flux de chaleur latente et sensible au-dessus de la baie d'Hudson, entraînant une sous-estimation de l'occurrence des ETCs. Enfin, le manque de détails orographiques dans les MCGs contribue à des biais notables dans la simulation des précipitations et des vents près de la surface (Evans & McCabe, 2013; Rummukainen, 2016).

Afin de pallier les limites de la résolution spatiale des MCGs, plusieurs approches complémentaires ont été développées. L'une d'elles, regroupée dans le cadre du *High Resolution Model Intercomparison Project* (Haarsma et al., 2016; Roberts et al., 2025), s'appuie sur des MCGs atmosphériques dont la maille horizontale de la grille globale est de l'ordre de 25 à 50 km. Une autre approche largement utilisée consiste à appliquer une mise à l'échelle dynamique au moyen de modèles régionaux du climat (MRCs) (Giorgi, 2019; Laprise, 2008; Laprise et al., 2008). Ces derniers sont également intégrés aux projets CMIP par l'entremise du *Coordinated Regional Climate Downscaling Experiment* (CORDEX) (Giorgi & Gutowski, 2015; Giorgi et al., 2006; Jones et al., 2011). Ce principe repose sur l'exécution des simulations sur un sous-domaine géographique restreint, ce qui permet de raffiner la maille horizontale tout en maintenant une charge de calcul raisonnable.

Il est démontré dans la littérature que les simulations des MRCs améliorent la représentation de l'intensité des ETCs, principalement grâce à une simulation plus réaliste des processus de libération de chaleur latente (Willison et al., 2013; Zhang & Colle, 2018) et à une représentation plus précise de l'orographie (Jung et al., 2006). Par exemple, Seiler et al. (2018) ont appliqué une réduction d'échelle du modèle de système Terre CanESM2 au modèle régional CanRCM4, à une résolution horizontale de ~24 km le long de la côte est de l'Amérique du Nord. Ils ont observé une augmentation de la fréquence des ETCs à développement explosif, accompagnée d'une hausse de 22 % des précipitations. De plus, Booth et al. (2018) ont montré qu'un MRC à haute résolution simulait des précipitations associées aux ETCs supérieures à celles issues de produits de réanalyse ou de MCGs. Cette même étude suggère que cet écart résulte de cyclones plus intenses, avec des vents de surface plus rapides, favorisant une libération accrue de chaleur latente au sein du système.

Néanmoins, la simulation des ETCs avec les MRCs comporte également des défis, notamment avec les bordures latérales du domaine réduit ainsi que l'emploi de techniques de lissage spatial qui influencent les trajectoires des ETCs simulés près des bordures, mais aussi à l'intérieur du domaine (Côté et al., 2015). De plus, la quantité de précipitation simulée par les MRCs demeure sensible au choix du schéma de paramétrisation de la convection, ce qui introduit des biais persistants dans les champs de précipitation (Kendon et al., 2012; Lee et al., 2007; Tripathi & Dominguez, 2013). En ce qui concerne les vents à la surface, l'augmentation de la résolution horizontale permet l'amélioration de leur représentation spatiale, mais cette relation n'est pas linéaire et dépend des méthodes statistiques employées (Belušić et al., 2018; Schaaf & Feser, 2018). En effet, Belušić et al. (2018) a comparé les vitesses de vent journalières et aux trois heures de douze simulations, dont dix issues de MRCs suivant le protocole CORDEX ainsi que deux simulations provenant du MRC COSMOS (Leutwyler et al., 2016), réalisées à des résolutions horizontales de 0,44°, 0,11° et 0,02° sur les eurorégions adriatique et ionienne. L'analyse met en évidence une valeur ajoutée des simulations à 0,11° par rapport à celles à 0,44°, perceptible dans la médiane et l'intervalle interquartile de l'intensité du vent, alors qu'aucune amélioration n'est observée avec le score de performance de Brier (Brier skill score). Dans cette même étude, les simulations à 0,11° et 0,02° présentent des performances comparables, mais la résolution à 0,02° reproduit plus fidèlement les analyses spectrales sous-journalières, se situant à l'intérieur des incertitudes des observations.

Au cours de la dernière décennie, les modèles climatiques régionaux à représentation explicite de la convection (MRCCEs) se sont imposés comme des outils prometteurs pour la production de projections

climatiques à très haute résolution (< 4 km). À cette échelle, la résolution horizontale devient suffisante pour représenter explicitement la convection profonde, réduisant ainsi la dépendance aux schémas de paramétrisation (Lucas-Picher et al., 2021). Les MRCCEs ont démontré leur capacité à améliorer la représentation des champs de surface, notamment en capturant plus fidèlement les effets locaux des vents (Belušić et al., 2018; Cholette et al., 2015) et l'intensité des précipitations (Ban et al., 2021; Berthou et al., 2020; Chan et al., 2020; Chang et al., 2020; Dai et al., 2020; Fosser et al., 2015; Prein et al., 2013). Sur le continent européen, plusieurs études se sont penchées sur la valeur ajoutée des MRCCEs pour la simulation des champs de surface associés aux cyclones extratropicaux. Par exemple, Leutwyler et al. (2016) ont montré dans une étude de cas de la tempête Kyrill de 2007 qu'une simulation à 2,2 km offrait une organisation plus cohérente de la convection imbriquée le long du front froid qu'une version à 12 km utilisant la paramétrisation de la convection profonde. De façon similaire, Schaaf et Feser (2018) ont raffiné la grille d'un MRC de 12 km à 2,8 km pour simuler la tempête Christian en Allemagne. En comparant les deux configurations aux observations de stations météorologiques, ils ont montré que le MRCCE présentait une valeur ajoutée pour la simulation de la précipitation convective et des vents près de la surface, telle que mesurée par le score de performance de Brier. Dans la même étude, une analyse multi tempêtes a révélé que le MRC avec convection paramétrée représentait de façon satisfaisante la direction du vent et les précipitations, ce qui suggère que les avantages des MRCCEs se manifestent surtout dans la simulation des champs aux échelles temporelles sous-journalières et spatiales locales. À ce jour, aucune étude n'a évalué en Amérique du Nord la valeur ajoutée des MRCCEs dans la représentation des précipitations et des vents de surface associés aux ETCs.

L'étude présentée dans ce mémoire vise à combler cette lacune dans les connaissances en évaluant la performance de la sixième version du Modèle régional canadien du climat (MRCC6-GEM5) pour la simulation des ETCs et des champs de surface associés, tels que la vitesse des vents près de la surface et la précipitation, au nord-est de l'Amérique du Nord. À cette fin, le MRCC6-GEM5 est utilisé avec deux résolutions horizontales : une version à ~12 km, qui emploie un schéma de paramétrisation de la convection profonde, et une version à ~2,5 km, qui la résout explicitement. Plus précisément, l'étude s'articule autour de deux sous-objectifs :

1. Les ETCs simulés sont identifiés et leurs trajectoires suivies à l'aide d'un algorithme lagrangien de suivi des cyclones, développé à l'UQAM et dont l'évaluation a fait l'objet de travaux préalables

(Chen et al., 2022). Leurs caractéristiques (fréquence, intensité et durée de vie) sont comparées à celles des ETCs extraits de la réanalyse ERA5.

2. Les champs simulés de précipitation et de vitesse du vent près de la surface associés aux ETCs sont évalués à partir d'observations, en mettant particulièrement l'accent sur la valeur ajoutée de la version à 2,5 km. L'évaluation des champs de surface repose sur des produits satellitaires, des données radar et des observations in situ.

Le mémoire est structuré comme suit : Le chapitre 1 présente un article scientifique rédigé en anglais, actuellement en préparation pour soumission au Journal of Geophysical Research Atmospheres du American Geophysical Union. La section 1.2 décrit les configurations du modèle utilisées ainsi que des jeux de données de référence. La section 1.3 présente le cadre méthodologique, incluant les régions et périodes d'étude. Les résultats relatifs aux trajectoires des ETCs et à leurs caractéristiques sont présentés dans la section 1.4.1, suivis de l'analyse des champs de surface associés dans la section 1.4.2. La section 1.5 propose une discussion des résultats, abordant notamment la fiabilité des produits de référence et la comparaison avec la littérature. Enfin, la section 1.6 présente les conclusions générales. Cinq annexes complètent le document et visent à fournir des informations supplémentaires pour l'article: l'annexe A présente la distribution saisonnière de la durée de vie des ETCs, l'annexe B porte sur la distribution des taux de précipitation de faible intensité, l'annexe C présente la distribution saisonnière des taux de précipitation et de vents au-delà d'un seuil défini, l'annexe D contient une discussion sur la sensibilité au choix de seuil pour le taux de précipitation et l'annexe E présente les champs de la vitesse du vent normalisée des produits utilisés.

CHAPITRE 1

ÉVALUATION DE LA PERFORMANCE DU MODÈLE RÉGIONAL CANADIEN DU CLIMAT POUR SIMULER LES CYCLONES EXTRATROPICAUX AU NORD-EST AMÉRIQUE DU NORD

Ce chapitre est présenté en anglais sous la forme d'un article scientifique. La rédaction de l'article, les figures et les analyses ont été réalisées sous la supervision de mes codirecteurs de recherche Alejandro Di Luca (Université du Québec à Montréal), Dominic Matte (Ouranos) et Philippe Roy (Hydro-Québec). L'article est en cours de préparation pour une soumission au Journal of Geophysical Research Atmospheres du American Geophysical Union.

EVALUATION OF THE PERFORMANCE OF THE CANADIAN REGIONAL CLIMATE MODEL IN SIMULATING EXTRATROPICAL CYCLONES OVER NORTHEASTERN NORTH AMERICA

Maxine Cloutier-Gervais[1], Alejandro Di Luca[1], Dominic Matte[2,1], Philippe Roy[3]

[1]Centre pour l'Étude et la simulation du climat à l'échelle régionale (ESCER), Département des sciences de la Terre et de l'atmosphère, Université du Québec à Montréal (UQAM), Montréal, Québec, Canada, [2]Ouranos, Montréal, Québec, Canada, [3]Hydro-Québec, Montréal, Québec, Canada

Corresponding author : Alejandro Di Luca, di_luca.alejandro@uqam.ca

ABSTRACT

The capacity of convection-permitting regional climate models to simulate extratropical cyclones (ETCs) and associated near-surface wind speeds and precipitation remains insufficiently explored. This study provides the first evaluation of the sixth version of the Canadian regional climate model (CRCM) for this purpose over Northeastern North America. Two CRCM configurations are analyzed : a ~12-km grid mesh with parameterized deep convection, driven by the ERA5 reanalysis, and a nested ~2.5-km convection-permitting version. ETCs are identified and tracked using a Lagrangian storm tracking algorithm, and storm trajectory, intensity and lifetime are evaluated against ERA5. Simulated ETC-associated near-surface wind speeds and precipitation are compared with in situ stations (ISD), satellite (IMERG), and radar (StageIV) observations over a common northeastern United States region. The 12-km simulation reproduces cyclone tracks and lifetimes comparable to ERA5, whereas the 2.5-km version generates more frequent and longer-lasting storms. Both configurations capture the main characteristics of ETC-associated surface fields, but the 2.5-km model better represents extreme precipitation rates and reduces wind speed biases. Bias decomposition of surface field indicates that discrepancies arise primarily from the intensity field during ETC events, and that a higher storm frequency does not necessarily yields greater precipitation totals. Overall, both configurations reasonably reproduce ETC characteristics, but the convection-permitting 2.5-km version is better suited for local-scale climate analyses.

1.1 Introduction

Extratropical cyclones (ETCs) are a key feature in the global circulation and moisture transport in the midlatitudes (Catto et al., 2019), delivering the majority of annual total precipitation across the Northern Hemisphere (Hawcroft et al., 2012). In addition to their vital role in midlatitude climatology, these synoptic-scale systems are the primary drivers of extreme wind and precipitation events (Booth et al., 2015; Chen & Di Luca, 2025; Pfahl & Wernli, 2012), often causing significant damage to both human infrastructures and ecosystems (Ashley & Black, 2008; Sibley, 2010). For instance, in northeastern North America, over 60% of extreme precipitation events throughout the year are associated with ETCs (Chen & Di Luca, 2025; Pfahl & Wernli, 2012). Moreover, Booth et al. (2015) identified winter high-wind events along the US east coast as instances when wind speeds exceeded 1-, 3-, or 5-year return levels and found that more than 80% of these events coincided with the passage of an ETC. A notable case of a synoptic storm that impacted northeastern North America is the 2019 Halloween Storm, which caused over CAD $250 million in insured damages in Canada, with wind gusts exceeding 100 km/h along the east coast and rainfall totals surpassing 100 mm in some parts of southern Quebec (Insurance Bureau of Canada, 2019). In a warming climate, these ETC-associated hazards are expected to evolve. For instance, ETC-related precipitation is projected to increase (Hawcroft et al., 2018; Zappa, Shaffrey, & Hodges, 2013), and shifts in ETC trajectories could drive substantial changes in local extreme wind speeds (Li et al., 2014; Priestley & Catto, 2022; Seiler & Zwiers, 2016; Zappa, Shaffrey, Hodges, et al., 2013). These projected changes reinforce the importance of producing reliable projections of their frequency and intensity to understand better how ETCs and the hazards they bring may evolve in the coming decades.

The dynamical intensity of ETCs is typically quantified using metrics such as vorticity, mean sea level pressure (MSLP), or near-surface wind fields derived from reanalysis or climate models (Seiler et al., 2018; Zappa, Shaffrey, & Hodges, 2013). There is a consensus in the literature that the coarse horizontal resolution of global CMIP-type global climate models (GCMs) leads to a systematic underestimation in ETC intensity (Colle et al., 2013; Di Luca et al., 2016; Jiaxiang et al., 2020; Priestley et al., 2020; Seiler et al., 2018; Trzeciak et al., 2016; Zappa, Shaffrey, & Hodges, 2013). The coarse resolution also limits the accurate representation of orography, further contributing to precipitation biases and surface winds in GCMs (Evans & McCabe, 2013; Rummukainen, 2016).

To overcome the spatial resolution limitations of global climate models (GCMs), complementary approaches have been developed. One of these, grouped under the High Resolution Model

Intercomparison Project (HighResMip) (Haarsma et al., 2016; Roberts et al., 2025), relies on atmospheric GCMs with refined global grids featuring horizontal resolutions on the order of 25–50 km. Another widely used approach consists of applying dynamical downscaling through the use of regional climate models (RCMs) (Giorgi, 2019; Laprise, 2008; Laprise et al., 2008). These models are also incorporated into CMIP initiatives through the Coordinated Regional Climate Downscaling Experiment (CORDEX) (Giorgi & Gutowski, 2015; Giorgi et al., 2006; Jones et al., 2011). The principle of dynamical downscaling is to perform simulations over a geographically limited subdomain, allowing the horizontal grid to be refined while maintaining a realistic computational cost.

Previous studies have demonstrated that RCM simulations improve the representation of ETC intensity, mainly due to a more realistic simulation of latent heat release processes (Willison et al., 2013; Zhang & Colle, 2018) and a more accurate representation of orographic effects (Jung et al., 2006). For example, Seiler et al. (2018) downscaled the ~313 km horizontal grid-spacing earth system model CanESM2 GCM with the ~24-km CanRCM4 over the North American Atlantic coast and reported an increase in the frequency of explosive ETCs by one third, accompanied by a 22% increase in precipitation. Similarly, Booth et al. (2018) found that the 20-km resolution RCM simulated the highest ETC-associated precipitation over the North Atlantic when compared to coarser-resolution reanalysis and GCM products, and suggested that this resulted from dynamically more intense cyclones, with stronger near-surface winds enhancing latent heat release. Nevertheless, simulating ETCs with RCMs also presents several challenges, particularly those related to the lateral boundaries of the limited-area domain and the use of spatial smoothing techniques, which can influence the trajectories of simulated ETCs not only near the boundaries but also within the interior of the domain (Côté et al., 2015). Moreover, the amount of precipitation simulated by RCMs still depends on the choice of convection parameterization schemes, which introduces persistent biases in precipitation fields (Kendon et al., 2012; Lee et al., 2007; Tripathi & Dominguez, 2013).

Over the past decade, convection-permitting regional climate models (CPRCMs) have emerged as a promising tool for producing fine-resolution (< 4 km) simulations, where the resolution becomes high enough to allow deep convection to be explicitly represented, reducing the impact of parameterization schemes (Lucas-Picher et al., 2021). Since then, CPRCMs have largely been proven to improve the representation of surface fields, including small-scale wind features (Belušić et al., 2018; Cholette et al., 2015) and precipitation intensity (Ban et al., 2021; Berthou et al., 2020; Chan et al., 2020; Chang et al., 2020; Dai et al., 2020; Fosser et al., 2015; Prein et al., 2013). Moreover, a few studies focused on the added

value of CPRCMs in simulating ETC-associated surface fields in Europe. For instance, in a case study of the 2007 Krill storm, Leutwyler et al. (2016) found that the CPRCM at a 2.2 km horizontal grid spacing simulation exhibited a more coherent organization of embedded convection near and along the associated cold front than the 12 km simulation with parameterized deep convection. Similarly, Schaaf and Feser (2018) downscaled a 24-km RCM simulation using a 2.8-km CPRCM version and studied the 2013 Christian storm over Germany. They compared both simulations to in-situ station observations and found that the CPRCM simulation provided added value in reproducing convective precipitation and 10-m wind speeds, as quantified by the Brier Skill Score. A multi-storm analysis in the same study showed that the primary benefits of CPRCMs lies in their improved performance at sub-daily and more localized spatial scales. To the best of our knowledge, however, no studies over North America have yet evaluated whether explicitly representing deep convection improves ETC-associated wind and precipitation fields.

This study aims to fill this gap by assessing the performance of the sixth version of the Canadian regional climate model (CRCM6-GEM5) in simulating ETCs and their associated surface fields (10-m wind speed and precipitation) over North America. We use the CRCM6-GEM5 with two horizontal grid meshes: a ~12 km version that uses parameterized deep convection and a ~2.5 km version that explicitly resolves deep convection. Specifically, the aim of this study is structured around two objectives :

1. Simulated mid-latitude cyclones are identified and tracked using a Lagrangian storm tracking algorithm (Chen et al., 2022), and their characteristics (e.g., frequency, intensity and duration) are compared to those identified and tracked using the ERA5 reanalysis.
2. Simulated ETC-associated 10-m winds and precipitation fields are evaluated against observations, with particular attention to the added value by the 2.5-km model version compared to the 12-km version. The evaluation of the simulated ETC-associated surface fields is performed using multiple in-situ, radar and satellite-based observed datasets.

The study is structured as follows. In Section 1.2, we introduce the model configuration and reference datasets. In Section 1.3, we describe the region, period and methodological framework. Results related to ETC trajectories and characteristics are presented in Section 1.4.1, followed by ETC-associated surface fields in Section 1.4.2. A discussion of the results, including the limitations of the reference datasets and comparisons with the literature, is provided in Section 1.5. Conclusions are drawn in Section 1.6.

1.2 Data

1.2.1 CRCM6-GEM5 simulated data

The CRCM6-GEM5 model is currently being developed at the ESCER (Étude et simulation du climat à l'échelle régionale) Centre at the Université du Québec à Montréal (UQAM), in collaboration with Environment and Climate Change Canada (ECCC) and the Ouranos Consortium. The CRCM6-GEM5 used here is based on version 5.0.2 of the fifth-generation Global Environmental Multiscale Model (GEM5) (Côté et al., 1998; McTaggart-Cowan et al., 2019a), developed by the Recherche en Prévision Numérique (RPN) group at ECCC. GEM5 serves as the operational numerical weather prediction model used by the Meteorological Service of Canada. The CRCM6-GEM5 model has been used in multiple other studies (Roberge et al., 2024; Veilleux et al., 2025; Whittaker et al., 2025).

Two configurations of the model are employed, differing in horizontal grid spacing and the choices of parameterization schemes. The first configuration, referred to as RCM12, utilizes a horizontal grid spacing of 0.11° (or ~12 km) over a domain that covers the CORDEX North American domain (see orange region in Figure 1.1). RCM12 is driven hourly by the ERA5 reanalysis and has 71 vertical levels with a model lid at 10 hPa. As described in Roberge et al. (2024), spectral nudging is applied to temperature and horizontal winds above the 0.85 hybrid level (~850 hPa), and for horizontal scales greater than 200 km, with a relaxation timescale of 8 h. The simulation employs a shallow convection scheme (Bechtold et al., 2001), which does not contribute to precipitation formation. Precipitation in RCM12 is generated through two mechanisms by the Kain-Fritsch deep convection scheme (Kain & Fritsch, 1990; McTaggart-Cowan et al., 2019b) and by the explicit condensation of water vapour through the Predicted Particle Properties (P3, version 3.1.6.4) microphysics scheme (Milbrandt & Morrison, 2016; Morrison & Milbrandt, 2015; Morrison et al., 2015). The P3 microphysics scheme constitutes a more sophisticated scheme compared to the one used in previous versions of the model (Martynov et al., 2013; Šeparović et al., 2013), and uses eight prognostic variables to simulate the formation and growth of cloud droplets and ice particles, allowing interactions between the two phases through mechanisms such as vapour deposition, aggregation and rimming. Precipitation is generated when particles grow large enough and eventually fall out of the cloud. Additionally, P3 incorporates a subgrid cloud and precipitation fraction scheme to improve the sensitivity to the model resolution (Chosson et al., 2014; Jouan et al., 2020). The dataset is available at an hourly temporal resolution, covering the period from January 1979 to April 2023.

The second configuration of the model, referred to as RCM2.5, uses a 0.0225° grid spacing (approximately 2.5 km). It is driven by the RCM12 simulation without spectral nudging and is run over the northeastern North America (NENA) domain (see green region in Figure 1.1). This configuration features 66 vertical levels, distributed in the same way as those in the RCM12 version but with a lower model lid at 25 hPa (Roberge et al., 2024). RCM2.5 is run with an explicit representation of deep convection. Consequently, in the RCM2.5 configuration, precipitation is generated explicitly through the P3 scheme or through the Kuo Transient shallow convection scheme (Bélair et al., 2005). This simulation was performed for the period from January 2012 to April 2023.

Both RCM12 and RCM2.5 simulations use version 3.6 of the Canadian Land Surface Scheme (CLASS) (Verseghy, 2000; Verseghy & MacKay, 2017) alongside the Freshwater Lake model (FLake) to represent surface lake temperatures (Martynov et al., 2012; Mironov et al., 2010). In both versions, near-surface wind speeds are derived using the Monin-Obukhov Similarity Theory (MOST), a function of the roughness length, the friction velocity and the stability in the surface layer. A more detailed description of near-surface winds in the CRCM6-GEM5 is provided in Whittaker et al. (2025). Both simulations provide various hourly variables, including the 850-hPa relative vorticity (VORT), MSLP, precipitation, and 10-m wind speed.

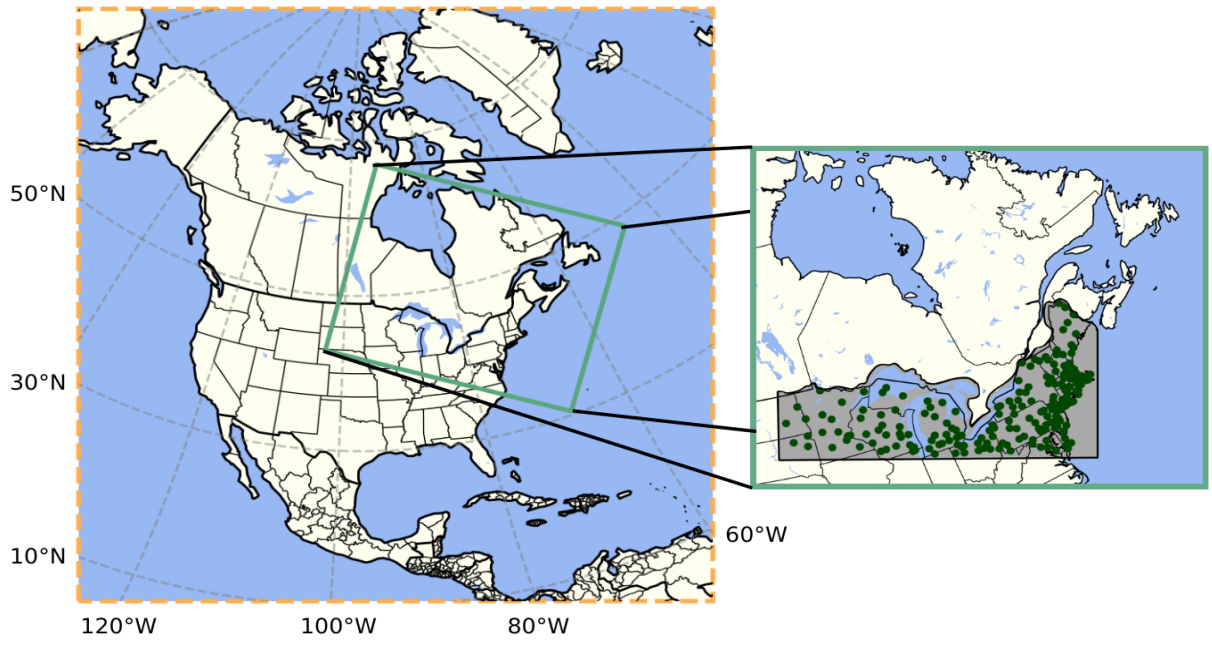

Figure 1.1 : Domain of the CRCM6-GEM5 simulation at 12 km (dashed orange) and 2.5 km (solid green) horizontal resolution. The northeastern United States domain is shaded in grey. Green dots indicate grid points used for analyzing ETC-associated 10-m winds and precipitation, selected based on hourly data availability in all variables from the ISD2ERA dataset (see Section 1.3.3).

1.2.2 ERA5 reanalysis data

ERA5 is the fifth-generation reanalysis product developed by the European Center for Medium-Range Weather Forecasts (Hersbach et al., 2020). ERA5 has consistently been used to evaluate RCMs in simulating near-surface wind speeds (Belušić Vozila et al., 2024; Coppola et al., 2024; ElBessa et al., 2021; Gurgel et al., 2024; Lakku & Behera, 2022) and precipitation fields (Bozkurt et al., 2021; Coppola et al., 2024; Karypidou et al., 2022). Hourly data is available on a global regular latitude-longitude grid with a horizontal grid spacing of 0.25° (approximately 31 km). It covers an extensive period from January 1940 to near real-time. Over the United States, ERA5 assimilates precipitation estimates from the National Centers for Environmental Prediction (NCEP) StageIV dataset (Lin & Mitchell, 2005), However, 10-m wind speed observations from surface stations across North America are not included in the assimilation process.

We extracted ERA5 VORT and MSLP fields to identify and track ETCs over North America. Then, 10-m wind speed and total precipitation fields are extracted to assess the model's capacity to reproduce high-impact variables associated with ETCs. Surface wind speed is calculated from the instantaneous (hourly) eastward (u) and northward (v) components of the 10-m wind, using the formula $ws = \sqrt{u^2 + v^2}$. Wind gust data is available in ERA5, but not in the other reference datasets used in the second part of the study. Consequently, only hourly near-surface wind speeds are evaluated here. Total precipitation over a grid box represents the hourly accumulation of liquid and solid water from both large-scale and parameterized convective precipitation.

1.2.3 10-m wind and surface precipitation observed data

Given the limitations of ERA5 in accurately representing high-impact local fields associated with ETCs, such as precipitation and surface winds (see Section 1.2.2), observational data will also be used to compare the results obtained from the RCM12 and RCM2.5 simulations. A total of three independent observational datasets, derived from satellites, radars, and surface weather stations, have been selected for this purpose (Table 1.1).

Table 1.1 : Summary of datasets used to evaluate ETCs-related wind and precipitation fields in the CRCM6-GEM5 model, including abbreviation, spatiotemporal resolution, domain, period, data sources, variables used and references.

Dataset	*Δx*	*Δt*	*Period*	*Domain*	*Type*	*Fields*	*Reference(s)*
ERA5	0.25 °	1 h	1979-2023	Global	Reanalysis	10-m winds, precipitation	Hersbach et al. (2020)
NEXRAD StageIV	4 km	1 h	2000-2022	CONUS	Adjusted radar, gauge	precipitation	Fulton et al. (1998) Lin and Mitchell (2005)
IMERG V07	0.1 °	30 min	200006-202312	Global	Adjusted satellite, gauge	precipitation	Huffman et al. (2020) Huffman et al. (2023)
ISD2ERA	0.25 °	1 h	1990-2021	North America	In Situ observations	10-m winds, precipitation	Collet et al. (2022) Chen et al. (2024)

The StageIV dataset (Lin & Mitchell, 2005) provides 4-km gridded observation data over CONUS. Precipitation estimates are generated through a mosaicking process that incorporates data from 12 National Weather Service River Forecast Centers. Precipitation estimates are generated from radar and precipitation gauge measurements by using the multi-sensor precipitation estimator and a field bias corrector (Nelson et al., 2016). Precipitation estimates from each River Forecast Center are then merged and biases are adjusted based on observations from hydrometeorological automated data system (HADS) gauges, automated surface observing system (ASOS) and automated weather station reports (AWOS) (Prat & Nelson, 2015). Data availability for StageIV was evaluated over 195 selected grid points over the northeastern United States, which are the only grid points from which StageIV data will be extracted (see Section 1.3.3). For each grid point, more than 99.8 % of the hourly records are available, which is considered sufficient for the purposes of this study.

NASA's Integrated Multi-satellitE Retrievals for Global Precipitation Measurement (GPM) mission produces the IMERG products, which estimate global surface precipitation rates at a spatial resolution of 0.1° every half-hour (Huffman et al., 2020; Huffman et al., 2023). The IMERG precipitation estimates integrate intercalibrated data from an international constellation of precipitation-relevant satellites, along with gauge analysis (Huffman et al., 2020). To ensure consistency across all datasets, the half-hourly data from IMERG has been converted to an hourly temporal resolution. Consequently, at a given time t, the accumulated precipitation reflects the total precipitation from the preceding hour, spanning from $t-1$ to t.

The North America Integrated Surface Database (ISD) to ERA5 (ISD2ERA5) Catalogue (Collet et al., 2022) is a station-based dataset of hourly 10-m wind speeds, surface total precipitation, mean sea level pressure and 2-m air and dew point temperature, covering the period from 1990 to 2021. The station observations are sourced from the ISD, which is developed by the National Oceanic and Atmospheric Administration's (NOAA) National Centers for Environmental Information (NCEI), and undergoes a series of rigorous quality checks (Chen et al., 2024; Smith et al., 2011). In this study, only the hourly surface wind speeds and accumulated precipitation will be used, derived from METeorological Aerodrome Reports (METARs) and NOAA's Climate Reference Network data. After undergoing a second series of quality checks and filtering processes, the data is interpolated onto the ERA5 grid using a nearest-neighbour method. For further information, readers are referred to Chen et al. (2024). Previous studies used the ISD2ERA dataset to evaluate near-surface wind speeds and precipitation from other products, including the ERA5 reanalysis (Chen et al., 2024) and IMERG (Chen & Di Luca, 2025).

1.3 Methods

1.3.1 Storm tracking algorithm

The period used in this study is from January 2012 to December 2022, covering the years common to both the reanalysis and the two model configurations. ETC centers are identified and tracked using a storm tracking algorithm developed at the ESCER center (Chartrand & Pausata, 2020; Chen et al., 2022). The domain of the tracking algorithm is bounded by latitudes 20°N to 80°N and longitudes 180°W to 0° (referred to as NA and shown in Figure 1.2). This domain encompasses North America, the North Atlantic, and the Eastern Pacific Oceans, capturing all ETCs that may affect North America. Synoptic storms are detected based on VORT and MSLP fields, which have been previously spatially smoothed using a 400-km radius Cressman filter to exclude small-scale local minima. An ETC is identified based on two criteria : the center must be a local minimum in the MSLP and the maximum smoothed VORT within a 200-km radius must be larger than 10-5s-1. This threshold has been used in other studies (Priestley et al., 2020). Cyclones lasting less than 24 h or travelling less than 1000 km are excluded. While this method filters out thermal lows and smaller systems, tropical cyclones may still be tracked, as no additional filter was applied to isolate mid-latitude cyclones.

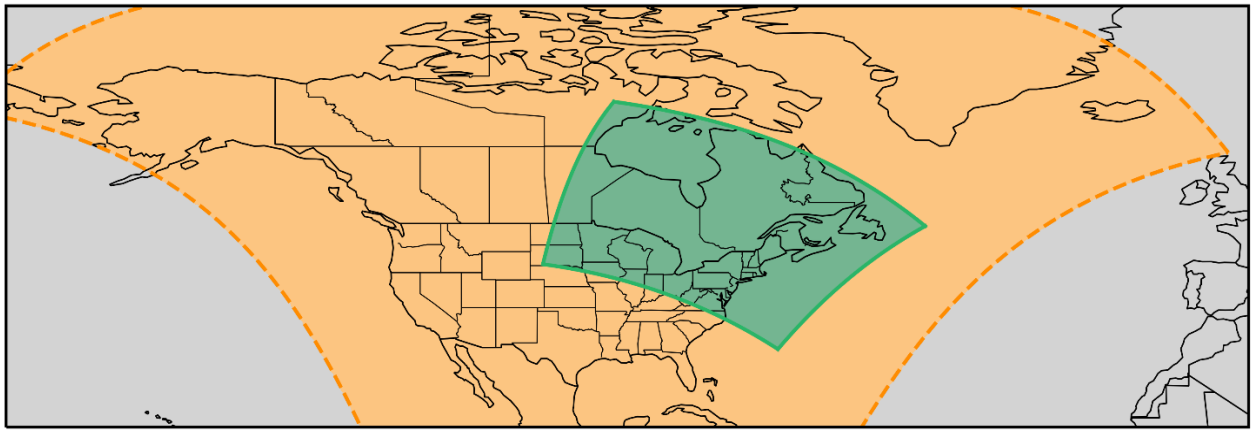

Figure 1.2 : North American (NA) domain used for extratropical cyclone tracking (solid black frame), with the RCM12 domain outlined in orange and the RCM2.5 domain in solid green. Data within the green area come from the 2.5-km version of the model interpolated onto the ERA5 grid, while data within the orange area come from the 12-km version, also interpolated onto ERA5 grid. In the grey area, values at a given grid point correspond to ERA5 data.

The storm tracking algorithm is applied to hourly, spatially smoothed VORT and MSLP fields from the ERA5 reanalysis, which will serve as the reference, and the two model simulations (RCM12 and RCM2.5). Before applying the algorithm to the two regional model simulations, we explicitly address the issue of discontinuous storm tracks near the lateral boundaries of the model domains by adopting the seamless method of Shkolnik and Efimov (2013). This method was adapted for the purposes of this study as follows :

1. The MSLP and VORT fields from RCM12 and RCM2.5 are conservatively interpolated onto the 0.25° regular latitude-longitude ERA5 grid.
2. All the grid points in the ERA5 solution that coincide with RCM12 grid points are replaced by the RCM12 solution for the corresponding time. Similarly, the RCM12 hourly solution is updated with the RCM2.5 solution at all coinciding grid points. Figure 1.2 provides a visual representation of this process.
3. The new merged RCM12 and RCM2.5 datasets are used as inputs for the storm tracking algorithm.

Due to the smooth transition between the driving data and the RCM, this method minimizes distortions at the lateral boundaries and enables the evaluation of a cyclone's complete life cycle as it enters a limited area. It also allows for the analysis of mesoscale forcings within the RCM domain (Shkolnik and Efimov, 2013). It is important to acknowledge the limitations of this approach. For instance, in a one-way nesting

configuration, cyclones that form within the RCM domain and move toward the lateral boundaries can pose challenges. Nevertheless, our analysis did not reveal any significant boundary artifacts.

1.3.2 Quantifying the intensity and lifetime of ETCs over northeastern North America

To analyze the intensity and lifetime of ETCs, the study focuses on the northeastern North America region (NENA), corresponding to the domain covered by the convection-permitting RCM2.5 simulation. We compared ETC lifetime and spatiotemporally averaged VORT from the RCM12 and RCM2.5 simulations against the ERA5 reanalysis. ETC intensity is quantified by averaging the smoothed VORT over a circular region centered on the cyclone, considering only the period during which its center remained within the RCM2.5 domain (Chen et al., 2022). A radius of 200 km is employed for this spatial averaging, similar to the 300 km radius used by Wang et al. (2023). We constrained our analysis to the NENA region in order to focus on the common domain to all three datasets. NENA storms must remain in the RCM2.5 domain, within a 5° distance from the lateral boundaries and for at least 24 consecutive hours (Chen et al., 2022).

1.3.3 Evaluating ETC-associated surface wind speed and precipitation over selected grid points

The need to use diverse observation datasets limits the ability to comprehensively evaluate the model over the whole northeastern North America region. For instance, StageIV radar data is not adjusted over Canada. Consequently, when evaluating ETC-associated precipitation and 10-m wind fields, the domain is further reduced to the Northeastern United States (NEUS), aligning with both the convection-permitting configuration and observations coverage (grey region in Figure 1.1). Even though the spatial spin-up belt is reduced with a double nesting approach (Roberge et al., 2024), grid points near the RCM2.5 domain's lateral boundaries were ignored to account for precipitation distortion in this region. Furthermore, since the ISD2ERA dataset is only available through December 2021, this part of the study will focus on the period from 2012 to 2021.

We evaluate the RCM's ability to represent the surface impacts of ETCs by comparing associated hourly wind speed and precipitation from RCM12 and RCM2.5 with ERA5 and observations over selected grid points in the NEUS domain. In fact, while our observational dataset ISD2ERA provides gridded data on the ERA5 regular grid, the fields originate from sparse in situ observations across the domain. As a result, the spatial and temporal gaps in the latter must be accounted for. To address missing values in ISD2ERA, a two-step filtering process was applied to all stations :

1. A given month at a grid point is retained if at least 90% of all five variables are available.
2. A station is retained if at least 90% of the months between 2012 and 2021 are considered valid.

Within the NEUS domain, this filtering process yields 195 valid stations, representing approximately 7 % of the initial 2821 ERA5 grid points. These selected points cover the entire NEUS domain, with higher densities along the U.S. East Coast (green points in Figure 1.1). To ensure a consistent comparison across observational, reanalysis and model products, the analysis of ETC-associated precipitation and surface winds is restricted to these 195 stations. To this end, all hourly surface wind and precipitation data from each dataset were interpolated onto the nearest station using a nearest-neighbor approach. This approach aims to reproduce what would be observed if the stations were embedded within the wind and precipitation fields of RCM12, RCM2.5, ERA5, IMERG V07 and StageIV datasets. Since the analysis is land-constrained, only the model and reanalysis grid points with a land-sea fraction greater than 90% were considered for the interpolation of the surface wind fields. To quantify ETC-related surface fields at these selected locations, hourly wind and precipitation fields are associated with an ETC center if the grid point lies within a 1000 km radius of a cyclone center (Field and Wood, 2007; Hawcroft et al., 2012). At each time step, observation and reanalysis fields are mapped to ETC tracks from ERA5, which serve as the reference for model evaluation. Similarly, hourly precipitation and wind fields from RCM12 and RCM2.5 are mapped onto their respective model-derived tracks.

1.3.3.1 Decomposing ETC-associated near-surface fields errors

To evaluate the ability of the simulations to reproduce ETC-associated near-surface fields, we apply a decomposition method inspired by Zappa et al. (2015) and Hawcroft et al. (2016). Specifically, we first consider the hourly precipitation rate (PR) and 10-m wind speeds (WS), larger than some threshold value θ, that are associated with ETCs at a given grid point (x, y) :

$$F_{ETC}^{\geq\theta}(x,y) = N_{ETC}(x,y) \cdot \mu_{F,ETC}^{\geq\theta}(x,y) \quad (1)$$

Where F represents either the cumulated ETC-associated precipitation or near-surface wind speed fields during the 2012-2021 period, $N_{ETC}(x,y)$ is the number of hours that the grid point (x,y) was affected by an ETC and $\mu_{F,ETC}(x,y)$ is the mean intensity of field F over those hours (i.e., $\mu_{F,ETC} = \frac{F_{ETC}^{\geq\theta}}{N_{ETC}}$). Equation (1) explicitly states that the cumulated variable $F_{ETC}^{\geq\theta}$ depends on both the number of ETCs and the number of events exceeding the threshold θ when an ETC is present. The choice of a threshold serves two purposes.

First, it enables a fairer comparison between observations and simulations, as some observational datasets struggle to detect low precipitation rates (e.g., station gauges may not record hourly precipitation below 0.2 mm). Second, it allows the evaluation to target a specific portion of the intensity distribution, such as the more extreme events.

Due to missing data in ISD2ERA (Section 1.3.3) and StageIV (Section 1.2.3), we normalize $F_{ETC}^{\geq\theta}(x,y)$ by N_{tot}, the total number of hours available in the dataset :

$$\hat{F}_{ETC}^{\geq\theta}(x,y) = \frac{F_{ETC}^{\geq\theta}(x,y)}{N_{tot}} = p_{ETC}(x,y) \cdot \mu_{F,ETC}^{\geq\theta}(x,y) \quad (2)$$

With $p_{ETC}(x,y) = \frac{N_{ETC}(x,y)}{N_{tot}}$, the probability of having an ETC at a given grid point. The terms $p_{ETC}(x,y)$ and $\mu_{F,ETC}^{\geq\theta}(\mathrm{x,y})$ can be calculated for simulations (p^m, μ^m) and for the reference datasets (p^r, μ^r). Finally, the error in the cumulated variable F can be decomposed into contributions from errors in p and μ (we have removed coordinates (x,y) for simplicity) :

$$\hat{F}_{ETC}^{\geq\theta,m} - \hat{F}_{ETC}^{\geq\theta,r} \quad = \quad \Delta\hat{F}_{ETC}^{\geq\theta} \; = \; p_{ETC}^{r} \cdot \Delta\mu_{F,ETC}^{\geq\theta} + \; \mu_{F,ETC}^{\geq\theta,r} \cdot \Delta p_{ETC} + \; \Delta\mu_{F,ETC}^{\geq\theta} \, \Delta p_{ETC} \quad (3)$$

Where the Δ term indicates the difference between simulated and observed values. Equation 3 illustrates that errors between the model and observation datasets stem from three terms:

1) $p_{ETC}^{r} \cdot \Delta\mu_{F,ETC}^{\geq\theta}$ is associated with discrepancies in the intensity of a given field during ETC events and is directly related to the ability of the model to simulate the field F when an ETC is present. This term is zero only when the model simulates the same field intensity as the reference dataset ($\mu_{F,ETC}^{\geq\theta,m} - \; \mu_{F,ETC}^{\geq\theta,r} = 0$).
2) $\mu_{F,ETC}^{\geq\theta,r} \cdot \Delta p_{ETC}$ arises from differences in the presence and location, including timing, of the ETCs themselves. For instance, a track may exist with ERA5 but not in the model (presence error), or the cyclone may follow a different trajectory, travel at a different speed, or appear and/or dissipate at different times (location and timing errors). Consequently, this term reflects the model's ability to reproduce the ETC trajectories and is only zero when the probability of ETC occurrence of the model is identical to the reference ($p_{ETC}^{m} - \; p_{ETC}^{r} = 0$).
3) $\Delta\mu_{F,ETC}^{\geq\theta} \, \Delta p_{ETC}$ is a cross-term error associated with interactions between both errors.

1.4 Results

1.4.1 Extratropical cyclone trajectories and characteristics

We begin by assessing the performance of RCM12 and RCM2.5 in simulating ETC trajectories and intensities over North America, with special attention to northeastern North America.

1.4.1.1 Cyclone tracks over North America

The spatial distribution of ETC center density in North America is shown in Figure 1.3. Here, density represents the percentage of ETC occurrences per time step and per unit area of 1000 km² at a grid resolution of 1.5° (Neu et al., 2013). Both RCM12 and RCM2.5 consistently simulate a higher density of cyclone centers over NENA, with the average relative differences being positive compared to ERA5 across all seasons. Notably, RCM2.5 systematically amplifies these differences relative to RCM12, especially during winter (DJF), where the average relative difference is five times higher for RCM2.5 than RCM12. The largest relative differences in cyclone center density are observed over land and during summer (JJA), reaching ~19 % for RCM12 and ~26 % for RCM2.5. During this season, RCM2.5 tends to simulate a higher density of ETC centers over southern Ontario and Quebec, while in DJF, it produces more centers around the periphery of the Hudson Bay region, including Northern Quebec and Ontario.

In total, ERA5 identified 6398 storms over the whole 2012-2022 period (Figure 1.4a). The RCM12 simulation detected 6410 ETCs, a number consistent with that of the reanalysis. Because the NA storm tracks were derived from RCM12 data for most of the domain, RCM2.5 also produced a similar total, identifying 6402 storms. Both the ERA5 and simulations agree with the distribution throughout the seasons, with more NA storms being identified over winter (1743, 1745 and 1751 for ERA5, RCM12 and RCM2.5) and fewer storms over summer (1364, 1424 and 1415, respectively).

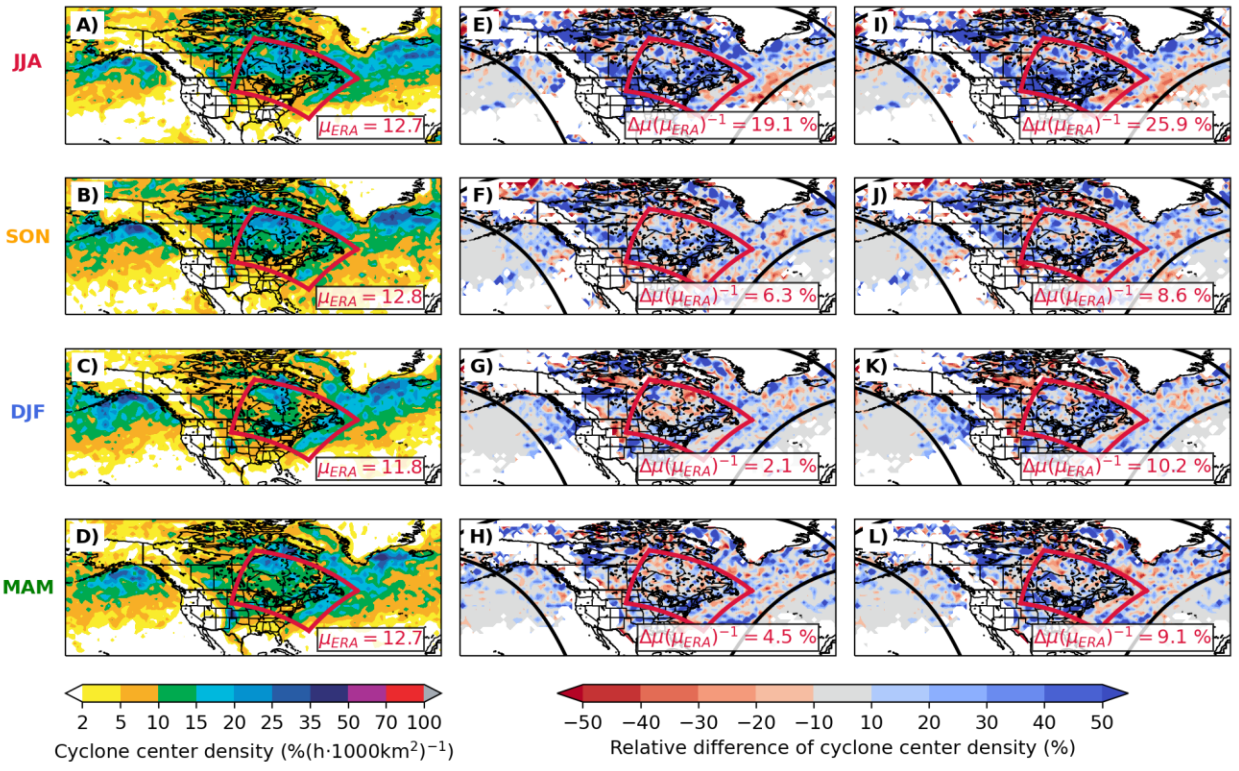

Figure 1.3 : ERA5 cyclone center density (A-D; per time step and unit area of 1000 km^2), along with relative differences between RCM12 and ERA5 (E-H) and RCM2.5 and ERA5 (I-L) for JJA (first row), SON (second row), DJF (second-to-last row) and MAM (last row). The solid black and red frames indicate the CRCM6-GEM5 model domains for the 12 km and 2.5 km simulations, respectively. Values in the lower right corner of each panel indicate the mean cyclone center density (first column) or mean relative difference (middle and last columns) over the red domain. Densities lower than 2 %(h.1000km^2)$^{-1}$ were ignored prior to relative difference calculations.

1.4.1.2 Cyclones over the northeastern North America (NENA) region

The analysis domain is then restricted to include only NENA storms (see section 1.3.2 for more details), yielding 926 storms for ERA5, 950 for RCM12 and 995 for RCM2.5, representing approximately 3% more ETCs for RCM12, and 7% for RCM2.5 (Figure 1.4b). The seasonal distribution of NENA storms is generally consistent between ERA5 and RCM12, with a peak in fall (245 storms in both datasets) and a minimum in summer (213 and 229 cyclones, respectively). In contrast, RCM2.5 simulated a higher number of ETCs than ERA5 and RCM12 across all seasons, particularly in winter and summer. While the minimum number of storm occurrences in RCM2.5 also occurs in summer with 241 storms, its winter count exceeds that of fall, differing from ERA5 and RCM12.

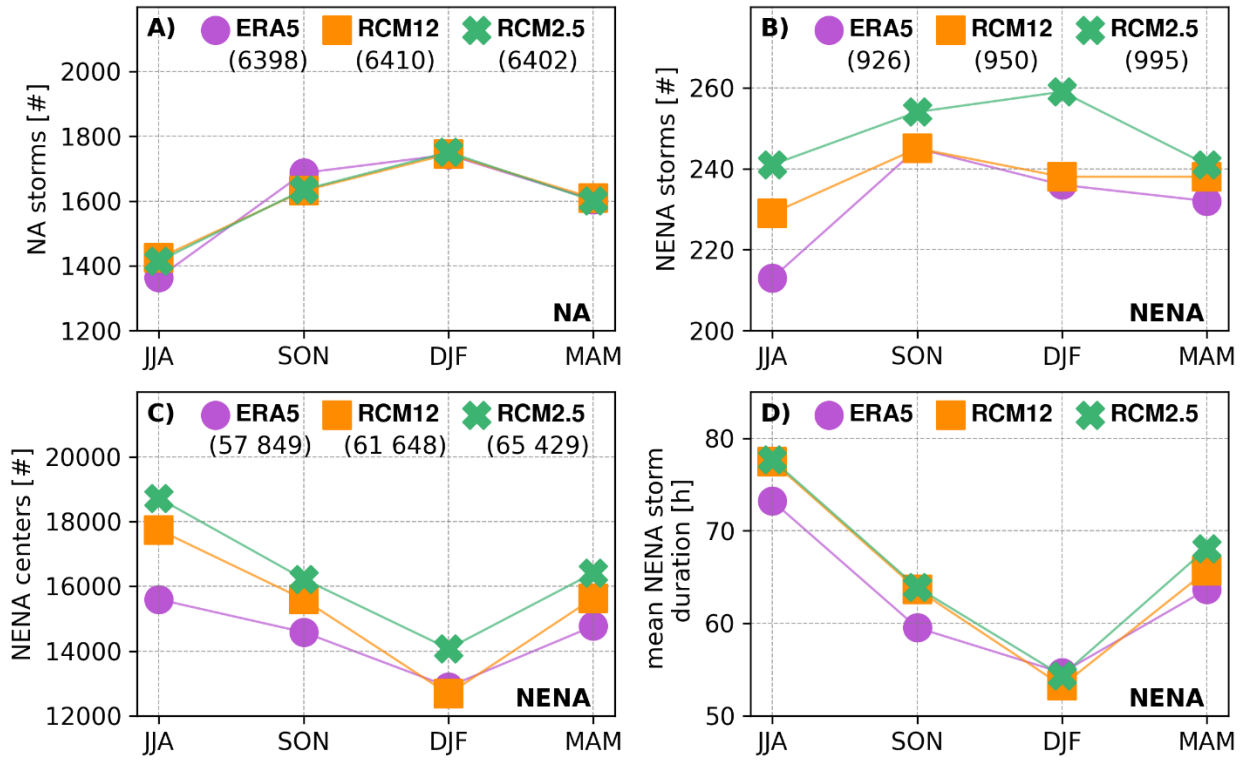

Figure 1.4 : Seasonal distribution of the total number of ETCs over the North American domain (A), the number of ETC retained after filtering over the northeastern North American (NENA) domain (B), the mean ETC duration in NENA (C) and the mean ETC duration (D). Mean ETC duration was calculated as the ratio of the total number of cyclone centers to the total number of NENA storms. Numbers in parentheses in (A)-(C) indicate the annual sum for each dataset.

The seasonal pattern of the total time storms spend in NENA is consistent across all datasets, with a maximum in JJA and a minimum in DJF (Figure 1.4c). However, there are differences in the magnitude of the duration. In JJA, RCM12 and RCM2.5 storms spend approximately 14 % and 20 % more time in NENA compared to ERA5, while in DJF, these differences shrink to about -2 % and 9 %.

To isolate storm lifetime from storm frequency, the total number of cyclone centers was normalized by the number of storms. Figure 1.4d shows that all datasets exhibit a similar seasonal pattern, with storms spending more time in NENA during summer and less during winter. This behaviour is consistent with the faster translation speed of ETCs in winter, driven by a stronger jet stream, and their slower movement in summer, when the 250-hPa winds weaken (Crawford et al., 2023). The normalized duration of RCM2.5 storms in NENA is about 6 % higher than ERA5 in JJA, while this difference shrinks to -1 % in DJF. This suggests that RCM2.5 may simulate more JJA storms that last for longer periods in NENA, whereas in DJF, it produces more storms with slightly shorter durations. This interpretation is supported by storm lifetime

distributions (Annexe A; Figure A.1), which show that in JJA, ERA5 storms spend an average of 73 hours in NENA versus 78 hours for RCM2.5; in DJF, average lifetimes are 55 hours for ERA5 and 54 hours for RCM2.5.

Lastly, we compare the simulated 850-hPa vorticity of NENA storms to that from ERA5 (Figure 1.5). All vorticities have been smoothed using the method described in Section 1.3.2. While this method ensures a fair comparison between all datasets, it may also suppress finer-scale features potentially introduced by the convection-permitting RCM2.5 simulation. All datasets exhibit similar results, with the weakest mean 200-km smoothed VORT during summer. Both ERA5 and RCM12 display the most intense vorticities during fall, while RCM2.5 rather yields the strongest vorticities in spring.

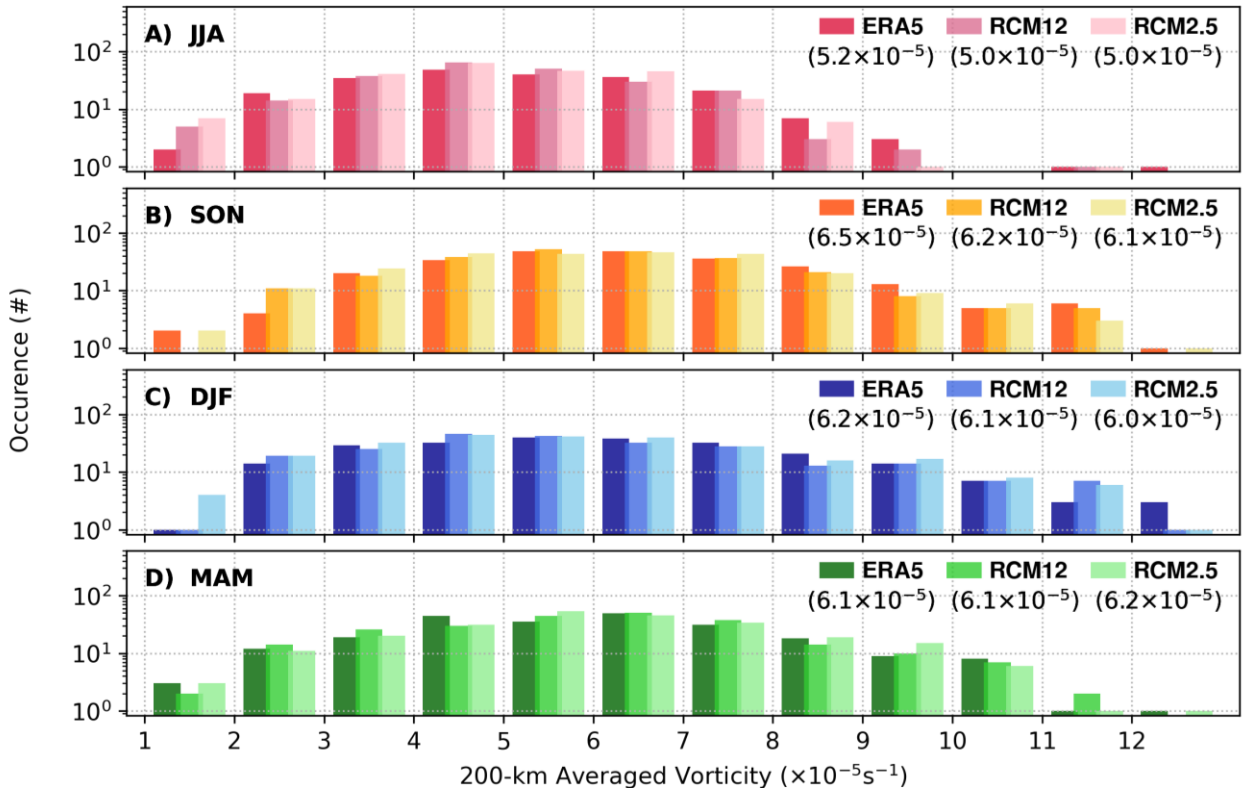

Figure 1.5 : Seasonal distribution of 850-hpa vorticity of extratropical cyclones within Northeastern North America (NENA) for ERA5, RCM12 and RCM2.5 during JJA (A), SON (B), DJF (C) and MAM (D). Vorticity fields are spatiotemporally averaged as described in Section 1.3.2. Mean values for each distribution of every dataset is displayed in the upper right quadrant.

1.4.2 ETC-associated surface fields over Northeastern United States

The second part of the study evaluates the performance of both RCM12 and RCM2.5 in simulating ETC-associated surface winds and precipitation. As outlined in Section 1.3.3, the analysis now focuses on the common NEUS domain, with results compared against the ERA5 reanalysis as well as the IMERG, StageIV and ISD2ERA observational datasets.

1.4.2.1 ETC-associated hourly precipitation

The largest discrepancies in the seasonal distribution of hourly ETC-associated precipitation occur at both the lower and upper extremes of the distribution (Figure 1.6). Across all seasons, ISD2ERA5 detects very few hourly values with low precipitation rates (below 0.2 mm h^{-1}), while both simulations and the ERA5 reanalysis exhibit a higher count of low precipitation rates than StageIV and IMERG. The distribution of precipitation rates below 1 mm h^{-1} (Figure B.1) is available in Annexe B to support these results.

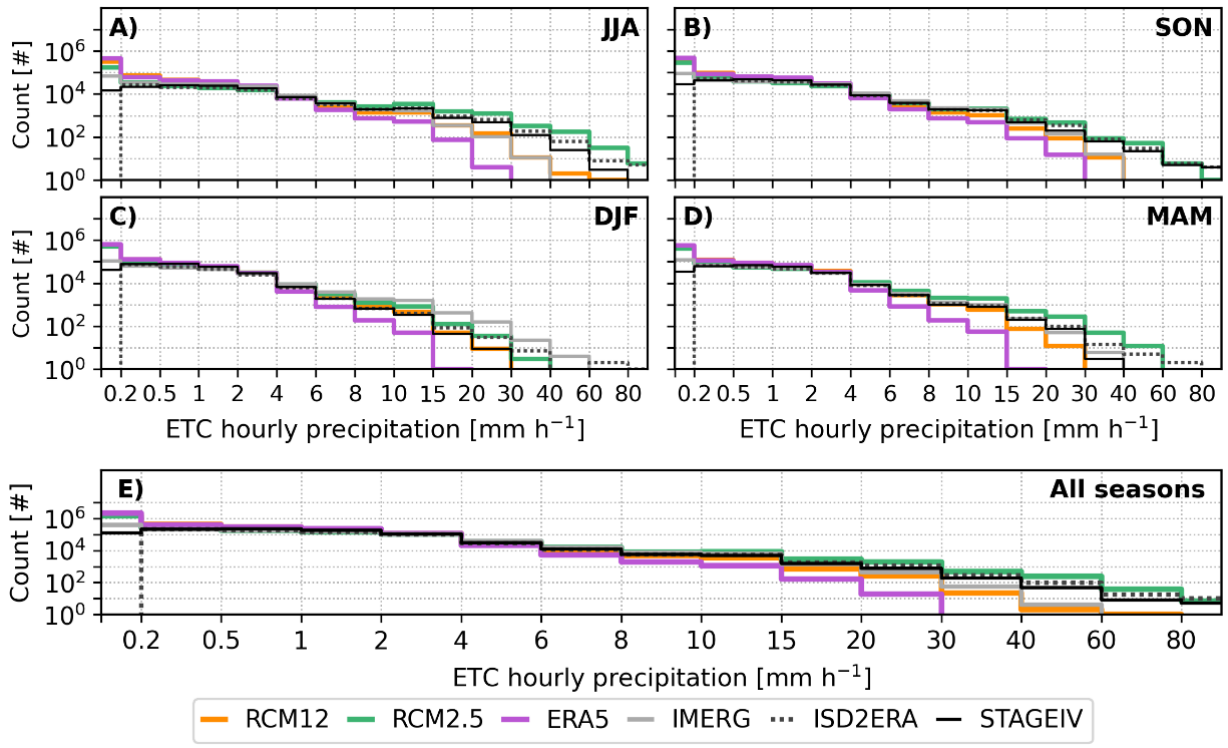

Figure 1.6 : Seasonal distribution of the count occurrence of ETC-associated hourly precipitation for JJA (A), SON (B), DJF (C), MAM (D) and all seasons combined (E) for RCM12 (orange) and RCM2.5 (green) simulations as well as ERA5 (purple), IMERG (gray), ISD2ERA (dashed black line) and StageIV (solid black line) reference datasets.

At the other end of the intensity distribution, ERA5 does not simulate precipitation rates exceeding 30 mm h^{-1}, significantly underestimating the most intense events compared to StageIV and ISD2ERA, which report values above 80 mm h^{-1}. According to ERA5, ISD2ERA and StageIV, the most extreme precipitation rates are typically observed in summer and fall, while winter and spring are associated with lower maxima. However, IMERG shows a different seasonal pattern, with higher maximum rates being more frequent in winter.

Regarding the simulations, RCM12 does not capture the most extreme rates observed by StageIV and ISD2ERA, but generally reproduces the correct seasonal pattern, with the highest rates occurring in summer and fall. All seasons combined, its distribution aligns most closely with IMERG, although notable underestimations are observed in winter with simulated rates reaching 30 mm h^{-1} versus 60 mm h^{-1} for IMERG. As for RCM2.5, the simulation reproduces frequencies of the most intense rates that are similar to those found in radar and in situ observations. It also agrees with the seasonal pattern but tends to overestimate the frequency of precipitation, particularly during summer and spring. For a more detailed analysis regarding the frequency distribution of extreme precipitation rates, see Annexe C (Figure C.1a).

Following the methodology described in Section 1.3.3.1, Figure 1.7 shows the decomposed error terms contributing to the total bias precipitation error. To maintain consistency among datasets, a threshold of θ = 1 mm h^{-1} is applied throughout the analysis. This threshold was selected because ISD2ERA does not detect light precipitation (< 0.2 mm h^{-1}) during ETC events (Figure 1.6), and further analysis (Appendix B) reveals eratic variability in ISD2ERA for rates below 1 mm h^{-1}. The resulting decomposition reveals that RCM12 underestimates the normalized total ETC-associated precipitation ($\Delta\widehat{PR}_{ETC}^{\geq\theta}$) when compared to IMERG and StageIV (Figure 1.7e-l), but overestimates it relative to ERA5 (Figure 1.7a-d) and ISD2ERA (Figure 1.7m-p). The term related to precipitation intensity biases ($p_{ETC}^{r} \cdot \Delta\mu_{F,ETC}^{\geq\theta}$) is the dominant contributor, primarily driving the underestimation relative to IMERG and StageIV and the overestimation relative to ERA5 and ISD2ERA. When compared to StageIV and ISD2ERA, RCM12 overestimates precipitation in the northern part of the domain, particularly along the Canada-US border and the northeast coast. In contrast, underestimations dominate over the southern and southwestern Great Lakes region. The term associated with ETC trajectory biases ($\mu_{F,ETC}^{\geq\theta,r} * \Delta p_{ETC}$) is positive at all stations. While its magnitude is generally smaller than that of the intensity term, the combined effect of both components helps either mitigate the total underestimation or amplify the overestimation in $\Delta\widehat{PR}_{ETC}^{\geq\theta}$.

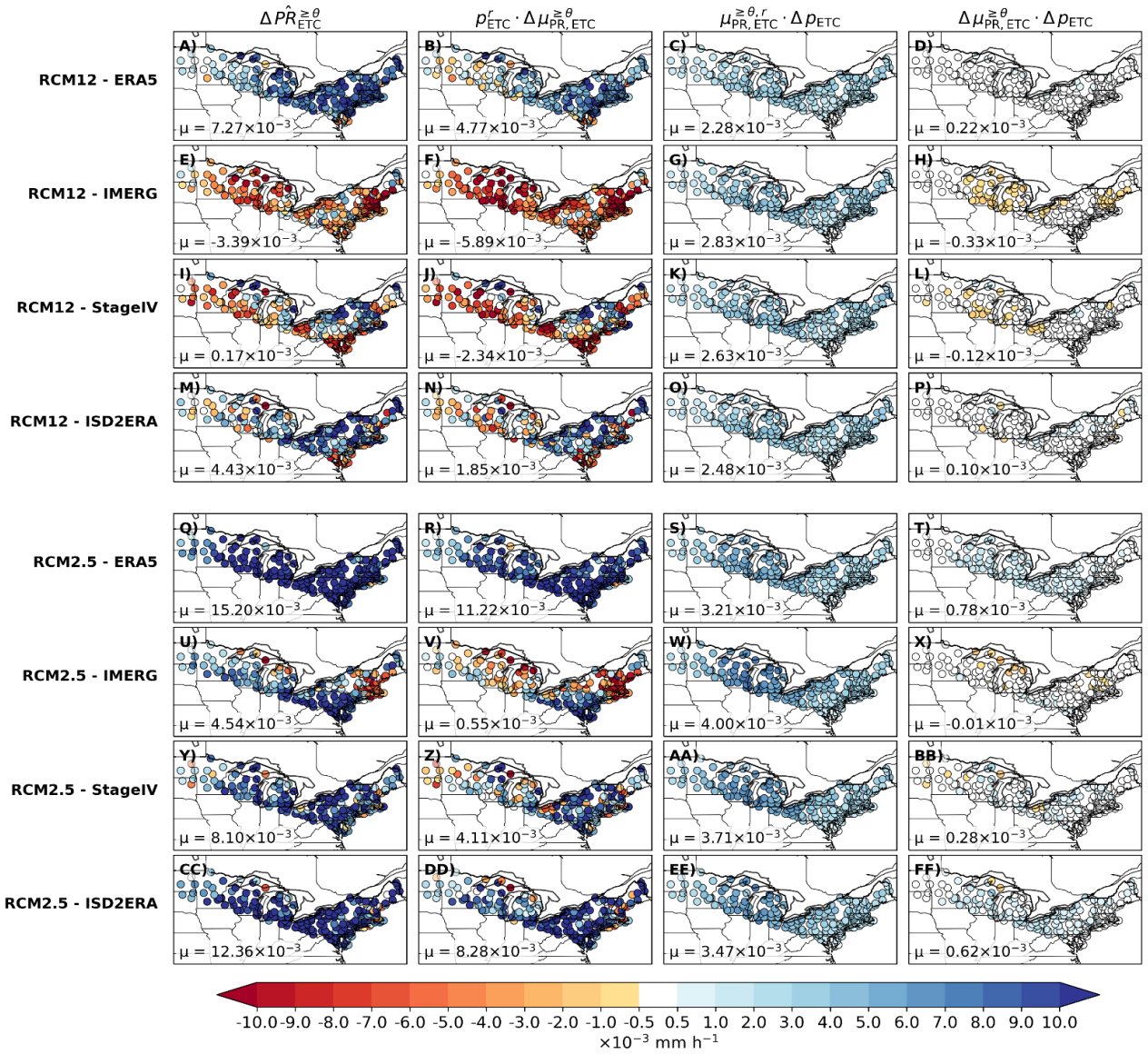

Figure 1.7 : Bias decomposition of normalized ETC-associated precipitation hourly (threshold θ = 1 mm h^{-1}) for RCM12 compared with ERA5 (A-D), IMERG (E-H), StageIV (I-L) and ISD2ERA (M-P) as well as for RCM2.5 compared with ERA5 (Q-T), IMERG (U,V), StageIV (Y-BB) and ISD2ERA (CC-FF). Each column corresponds to one term in Equation 6; column A-CC shows the total bias, column B-DD shows the precipitation intensity bias, column C-EE, the trajectory bias and D-FF, the cross-term bias. Numbers in the lower-left corner of each plot indicate the mean value across all stations.

As for RCM2.5, a clear overestimation is evident across all datasets. Nevertheless, some spatial variability is present when comparing to IMERG (Figure 1.7u), with underestimations along the northeastern coast and the Canada-US border near the Great Lakes. The dominant contributor of this pattern to the total bias is the precipitation intensity term, which also drives the spatial variability. The term associated with the ETC trajectory biases remains positive and contributes to amplifying the total bias. A comparison of the mean values of $\Delta\widehat{PR}^{\geq\theta}_{ETC}$ between RCM12 and RCM2.5 shows that the overestimation in RCM2.5 tends to

be larger than the biases from RCM12. This is particularly notable with ISD2ERA, where RCM12 exhibits a mean bias of around 4 %, increasing to nearly 12 % with RCM2.5.

To assess how simulations represent more intense precipitation, a threshold of 10 mm h-1 is applied. When focusing on higher intensity rates, the decomposition results show a clear and spatially consistent underestimation of the total ETC-associated precipitation by RCM12 across all reference datasets, except ERA5 (Figure 1.8). In contrast, RCM2.5 exhibits predominantly positive biases with some local and modest underestimations over grid points in the western part of the domain and the northeast coast when compared to IMERG. For both simulations and regardless of the reference dataset, the total bias is mainly driven by the precipitation intensity term, which accounts for more than 80 % of the total error in all cases. The mean absolute bias across all stations is larger for RCM2.5 than for the RCM12 simulation, even when compared to StageIV (more information about spatial representativity is given in Section 1.5.3). This indicates that the RCM2.5 simulation produces too much precipitation during ETC events, in agreement with the finding of an overestimation of the most extreme precipitation intensities.

1.4.2.2 ETC-associated surface winds

The same analysis is now extended to 10-m wind speeds associated with ETCs, using ERA5 and ISD2ERA as the reference datasets, as these are the only sources providing surface wind data. The strongest near-surface winds (exceeding 22 m s^{-1}) occur most frequently in winter and spring across all simulation and reference datasets, closely followed by fall. The occurrence of high-wind speeds in ERA5 is clearly underestimated, with winds not exceeding 20 m s^{-1} for the whole period, while ISD2ERA observes wind speeds above 24 m s^{-1} (Figure 1.9).

Both simulations generally reproduce the observed distribution of ETC-associated wind speeds, with seasonal differences. RCM12 tends to overestimate the frequency of higher wind speeds in all seasons except summer, where maximum simulated values barely exceed 18 m s^{-1} while observations reached speeds up to 22 m s^{-1}. The RCM2.5 convection-permitting simulation aligns more closely with the ISD2ERA distribution, although it slightly underestimates the count of stronger winds during summer, fall and winter. A more detailed analysis regarding the distribution of high ETC-associated wind speeds is available in Annexe C (Figure C.1b).

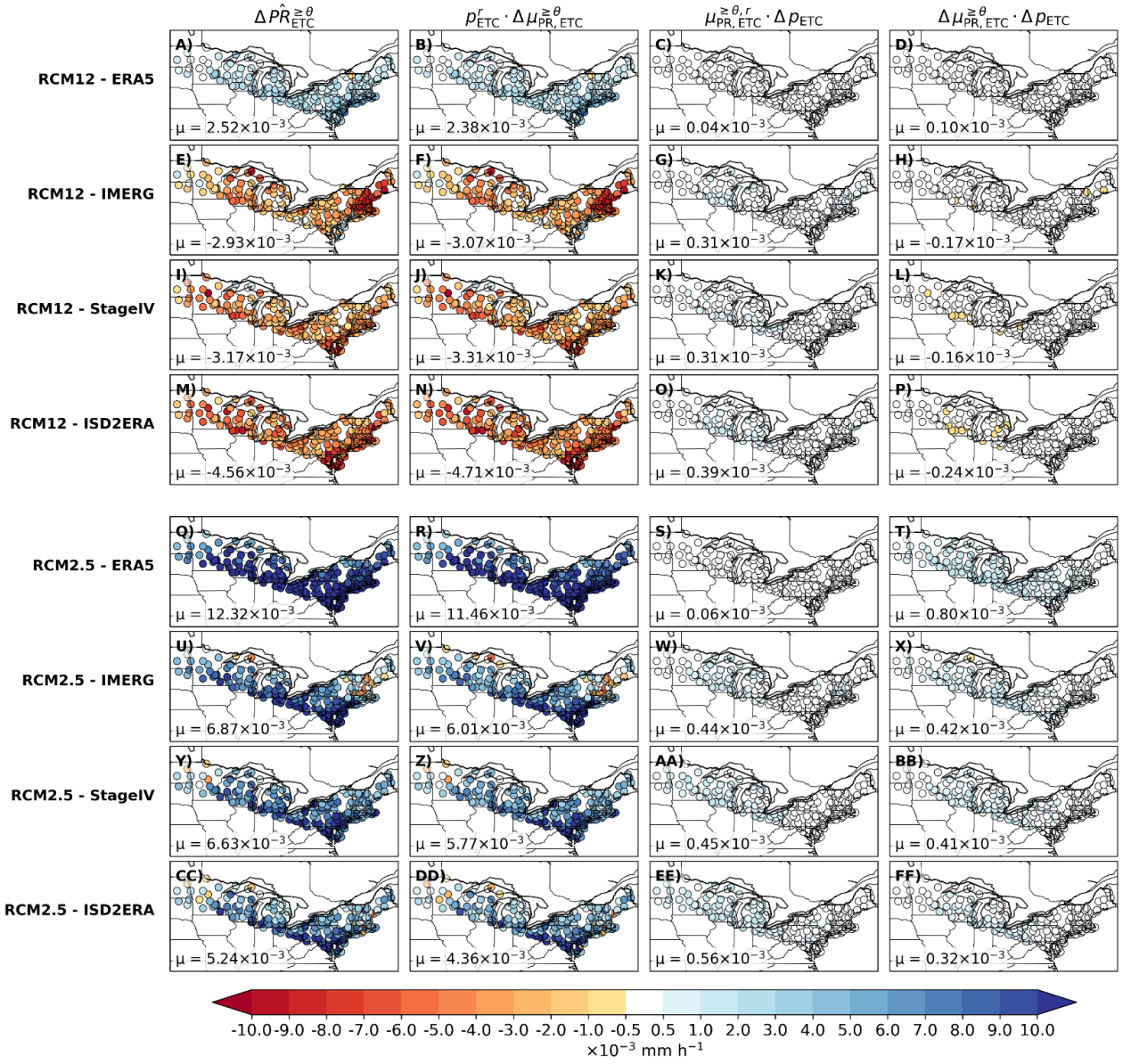

Figure 1.8 : Same as Figure 1.7, but with a threshold of θ = 10 mm h^{-1}.

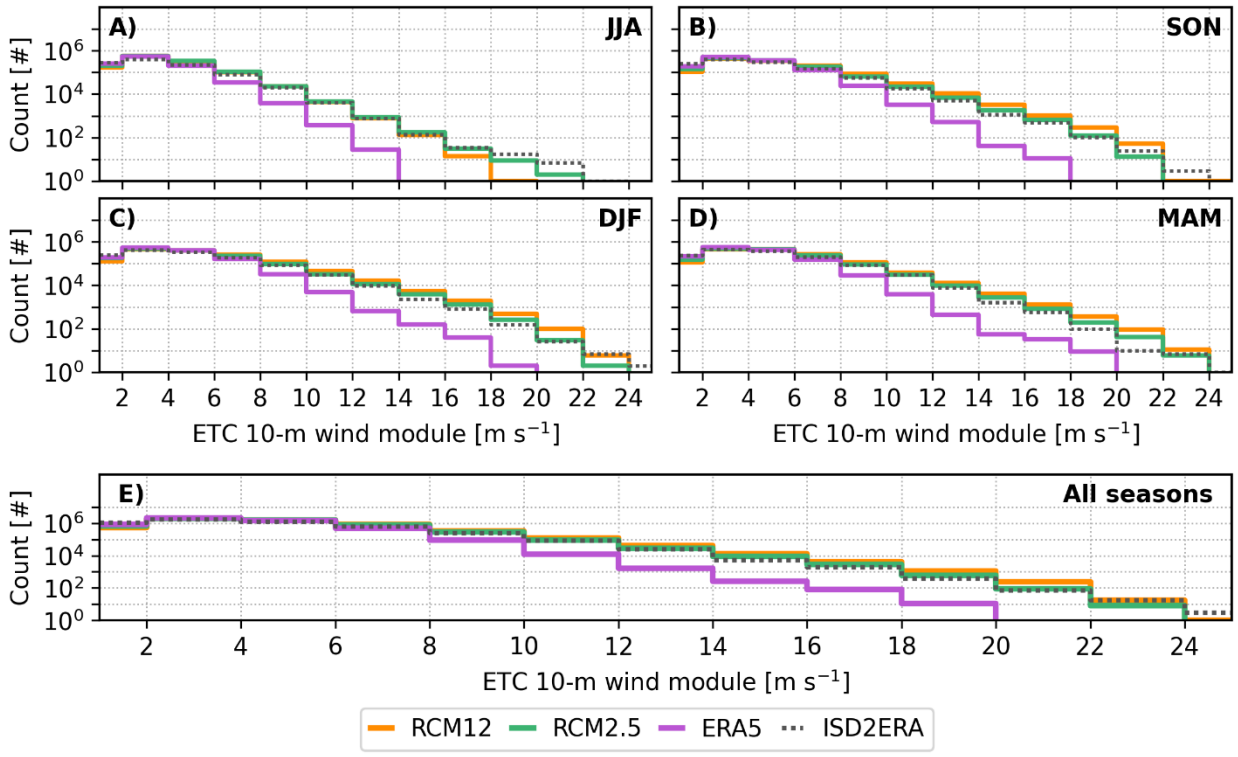

Figure 1.9 : Same as Figure 1.6 , but for the hourly ETC-associated wind speeds.

The same decomposition method used for ETC-associated precipitation is now applied to 10-m wind speeds by considering all values (Figure 1.10). As a result, simulations exhibit a general overestimation of ETC-associated wind speeds, with localized underestimations over the Great Lakes and the east coast when compared to ISD2ERA (e,m). The mean total error in ETC-associated wind speed is reduced with the convection-permitting simulation, indicating improved performance relative to RCM12. For the RCM12, the total bias is predominantly driven by errors in wind speed intensity, which accounts for more than 76 % of the total error. This term also dominates in the RCM2.5, contributing to 60 % and 67 % of the total error when compared to ERA5 and ISD2ERA, respectively. While the average ETC-frequency bias is higher in RCM2.5 than in RCM12 for both reference datasets, the opposite is observed for the wind speed intensity bias. Annexe E includes additional figures showing the individual normalized ETC-associated surface wind speeds for all datasets.

When only considering wind speeds higher than 10 m s^{-1} (i.e., using a threshold of θ = 10 m s^{-1}), the spatial variability in the total bias becomes more pronounced, especially in comparisons with ISD2ERA (Figure 1.11). For both model versions, more stations display negative biases, but large overestimations persist in

the southern and western parts of the domain, keeping the averaged total bias positive. Overall, the total bias pattern closely resembles that of the wind speed intensity term, with minimal influence from the ETC-frequency component. Finally, as observed for the 0 ms^{-1} threshold, RCM2.5 shows a smaller mean total bias than RCM12, and in both cases, the biases are lower when using ISD2ERA as a reference compared to ERA5.

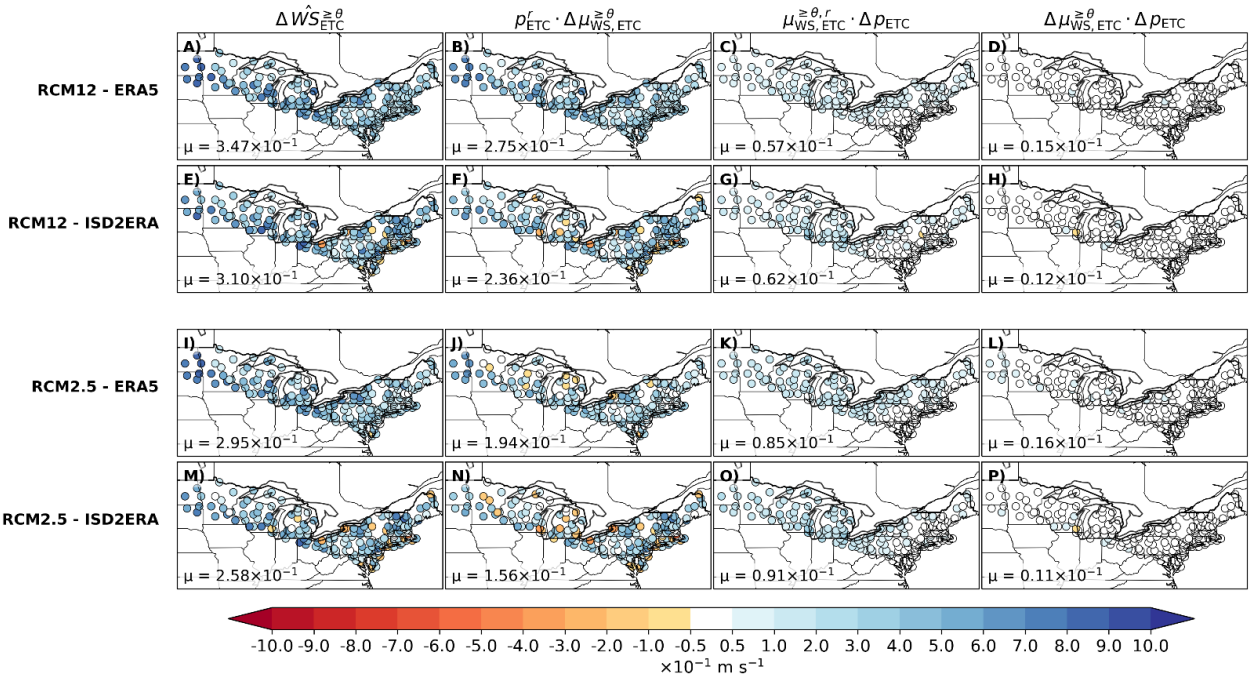

Figure 1.10 : Bias decomposition of normalized ETC-associated surface winds (threshold θ = 0 m s-1) for RCM12 compared with ERA5 (A-D), and ISD2ERA (E-H) as well as for RCM2.5 compared with ERA5 (I-L) and ISD2ERA (M-P). Each column corresponds to one term in Equation 6; column A-M show the total bias, column B-N show the wind speed intensity bias, column C-O, the trajectory bias and D-P, the cross-term bias. Numbers in the lower-left corner of each plot indicate the mean value across all stations.

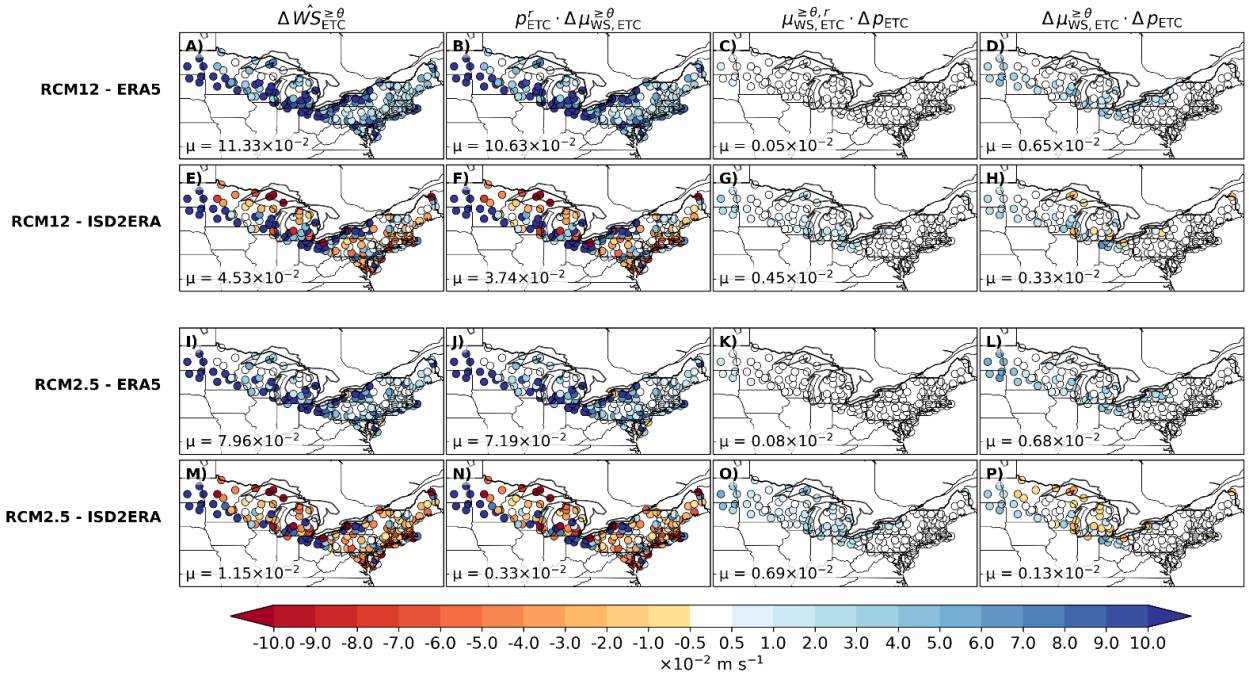

Figure 1.11 : Same as , with a threshold of θ = 10 m s^{-1}.

1.5 Discussion

1.5.1 Reference datasets

Consistent with this study, Chen and Di Luca (2025) found that ETC-related precipitation exceeding the 99th annual percentile occurs most frequently in summer and fall. However, given the presence of biases in reference datasets, these results should be interpreted carefully.

IMERG illustrates these limitations, as it exhibits a different seasonal behaviour and tends to overestimate precipitation rates in winter, resulting in a seasonal peak during the colder months. The recently released IMERG V07 (Huffman et al., 2023) has not yet been thoroughly evaluated for solid precipitation over the study region. However, studies using its predecessor, IMERG V06, indicate that its performance is temperature-dependent (Hosseini-Moghari & Tang, 2022) and that it overestimates hourly and 6-hourly precipitation during winter (Boisvert et al., 2021; Zhao et al., 2023). These findings suggest that wintertime comparisons involving IMERG should be interpreted with caution. Similarly, even if StageIV replicates the same seasonal pattern as ERA5 and ISD2ERA, studies report an underdetection of solid precipitation when compared with CloudSat Cloud Profiling Radar (Smalley et al., 2014) and rain gauges from the U.S. Climate

Reference Network (Nelson et al., 2021). Both studies indicate, however, that underestimations are less pronounced in cases of mixed and liquid precipitation.

Chen et al. (2024) assessed ERA5's performance in representing ETC-associated hourly 10-m wind speeds and precipitation over North America by comparing its output to hourly surface observations from the ISD station network. Using the normalized mean bias and the normalized root-mean-square error as evaluation metrics, they found that ERA5 performs well in reproducing spatially averaged 10-m wind speeds, but tends to underestimate high wind speeds and overestimate low ones. These limitations are taken into account in this study, particularly with regard to ERA5's reduced ability to capture localized extremes within ETCs.

The observed seasonality of ETC-associated winds is consistent with previous studies. Gilliland et al. (2020) conducted a climatology of windstorms over the eastern United States and reported a higher frequency of sustained high-wind events in winter and spring. Similarly, Letson et al. (2021) identified the 10 most extreme windstorms in the same region over the past four decades, nine of which were linked to extratropical cyclones occurring during winter or spring. Chen and Di Luca (2025) extracted ETC-associated near-surface wind speeds from the ERA5 reanalysis for the period 2001 to 2020 and found that in the northeastern US, extreme wind speed events (above the 99th percentile) occurred most frequently in winter, closely followed by spring and fall.

1.5.2 ETC storms and lifetime biases

Over NENA, previous studies have also highlighted that higher-resolution models tend to simulate more storms than reanalyses. Jiaxiang et al. (2020) found that cyclone frequencies increased in higher-resolution models in a hemispheric comparison between reanalyses and HighResMip simulations. Similarly, Di Luca et al. (2016) reported that a regional climate model ensemble over the Australian east coast produced a greater number of storms with longer lifetimes compared to the GCM ensemble mean.

We speculate that this positive relationship between model resolution and cyclone frequency is partially explained by enhanced latent heat processes in higher-resolution models and the representation of deep convection, whether it is parameterized or explicitly resolved. For instance, in a study on the sensitivity of summer cyclones to dynamical downscaling over North America, Zhang et al. (2019) reported that 30-km resolution simulations produced between 10 and 20 % more summer storms than coarser-resolution

GCMs. They also showed that the ETC frequency is strongly influenced by the choice of the convection scheme. In RCM12, the convection scheme may enhance latent heat release and vertical transport of sensible heat, thereby altering the thermodynamic structure of the atmosphere (Yanai & Johnson, 1993) and redistributing potential vorticity in a way that favours cyclone development (Lackmann, 2011). In the convection-permitting RCM2.5 simulation, we speculate that the absence of a deep convection scheme may further amplify latent heat effects, potentially leading to an even greater number and longer duration of JJA storms. The better agreement of the simulated (both RCM2.5 and RCM12) number of cyclones with ERA5 in winter compared to summer may reflect the reduced role of convection and latent heat during winter. It should be noted that the use of spectral nudging when driving the RCM12 with the ERA5 reanalysis prevents the 12-km simulation from substantially diverging from the reanalysis.

1.5.3 Spatial representativity of wind and precipitation

The evaluation of simulated precipitation and wind speeds relied on multiple observational datasets representing distinct horizontal spatial scales. Model output, radar-based (i.e., StageIV) and satellite-based (i.e., IMERG) products are generally interpreted as areal-mean values over the size of a grid cell box (Chen & Knutson, 2008; Di Luca et al., 2021). On the other hand, station data (i.e., ISD2ERA) is interpreted as point-based estimations. Therefore, a perfect agreement between model output and point-based observations does not imply a perfect performance of the model. For instance, considering hourly precipitation extremes, such an agreement would more likely reflect an overestimation by the model, since its values represent spatial averages over areas of 12 × 12 km for RCM12 and 2.5 km × 2.5 km for RCM2.5, and hourly extremes are expected to decrease as the representativeness area increases. A more robust evaluation of the model's performance is achieved by comparing RCM12 with IMERG (~10 km × 10 km) and RCM2.5 with StageIV (~4 km × 4 km), as these pairs of products share similar spatial resolutions and thus resolve features at comparable scales. The analysis in Section 1.4.2.1 illustrates that the RCM12 matches well with IMERG values most of the year, but in winter, when the IMERG performance is likely limited. The comparison between RCM2.5 and StageIV shows a generally good performance by the model, although it overestimates precipitation extremes, particularly during the summer season.

The absence of extreme precipitation rates in RCM12, relative to radar and in situ observations, does not necessarily indicate poor model performance, but rather reflects the inherent limitations of its coarser resolution. When compared with products of similar horizontal resolution, both simulations reproduce the total and hourly ETC-associated precipitation reasonably well, with RCM2.5 capturing higher precipitation

rates. The resolution mismatch poses a limitation for surface wind evaluation, as IMERG and StageIV do not provide wind observations. Despite this, comparisons with ISD2ERA indicate that while both simulations exhibit wind biases, the convection-permitting model reproduces ETC-associated winds more accurately. Overall, both model configurations perform well in simulating ETC-associated 10-m wind speeds and hourly precipitation, but the convection-permitting configuration is better suited for local impact studies due to its closer agreement with in situ measurements.

1.5.4 ETC-associated precipitation

Several studies have highlighted that CPRCMs tend to produce higher precipitation intensities than models with parameterized convection, particularly during summer months (Ban et al., 2021; Ban et al., 2014; Berthou et al., 2020; Chan et al., 2013; Fosser et al., 2015; Kendon et al., 2012; Lipzig et al., 2022). In particular, CPRCMs capture more convective and intense precipitation along cold fronts associated with extratropical cyclones, a feature that is generally absent when convection is parameterized (Leutwyler et al., 2016; Schaaf & Feser, 2018). These studies support the observed seasonal enhancement of extreme precipitation rates in convection-permitting simulations, especially in periods when convective processes dominate, with smaller differences reported during winter.

However, despite better agreement with observations, RCM2.5 tends to overestimate ETC-associated precipitation, with the mean positive biases exceeding the negative biases seen in RCM12. Some of the bias may stem from methodological limitations, particularly during the warmer months when convective processes dominate. The analysis is confined to 195 grid points over a relatively small meteorologically homogeneous domain, with uneven spatial coverage across the stations. Given the localized nature of convection, it is possible that some events are missed when interpolating gridded data to the nearest station. A further explanation is that RCM2.5 may generate excessive precipitation during ETC events due to enhanced diabatic processes. Willison et al. (2013) noted that higher resolution models exhibit stronger feedback between latent heat release and cyclone intensification, which can amplify precipitation rates. This appears to be the most likely explanation, as the decomposition analysis points to the precipitation intensity term as the primary driver of the bias. This result is also consistent with Hawcroft et al. (2016), who similarly found that biases in storm-associated precipitation were mainly attributed to errors in intensity. It could be argued that more intense precipitation during ETC events in the RCM2.5 simulation should lead to longer-lasting storms through latent heating feedbacks, which in turn could increase ETC frequency. While this relationship held true for most stations in the NEUS, some locations saw an

underestimation of the ETC-related precipitation intensity, even when a positive bias in ETC frequency was observed.

The precipitation threshold for the decomposition was selected to account for data availability in ISD2ERA. However, the RCM12 results are highly sensitive to this threshold, especially for low precipitation rates. When a lower threshold of 0.2 mm h^{-1} is used, the underestimation of ETC-associated precipitation becomes less pronounced, particularly when compared to IMERG and StageIV. This likely reflects the tendency of RCM12 to simulate a higher frequency of small precipitation rates (< 0.2 mm h^{-1}). Further details on the sensitivity to the precipitation threshold can be found in Annexe D.

1.5.5 ETC-associated surface winds

The differences between RCM12 and RCM2.5 are less pronounced for ETC-associated winds, but improvements are still evident with the convection-permitting simulation. Similarly, Schaaf and Feser (2018) reported that a simulation with parameterized convection already captured ETC-associated surface wind speeds reasonably well, yet found small added value with the convection-permitting simulation. This enhancement may stem from the finer resolution in RCM2.5, which allows for a more accurate representation of orography and localized wind features (Belušić et al., 2018).

1.6 Conclusion

This study evaluates the performance of the CRCM6-GEM5 model in simulating ETCs and their associated surface fields over Northeastern North America during the period 2012-2022. Two simulations with different horizontal grid meshes were analyzed: a ~12-km simulation (RCM12) with parameterized deep convection, driven by the ERA5 reanalysis, and a ~2.5-km simulation (RCM2.5) with explicit deep convection nested within the 12-km run. The simulated ETC trajectories, lifetimes and intensities were compared against the ERA5 reanalysis, while ETC-associated precipitation and 10-m winds were compared to ERA5 and multiple high-resolution observational datasets, including satellite-derived data from IMERG, radar data from StageIV and in situ station observations from the ISD.

Over Northeastern North America, the main findings regarding ETC trajectories, lifetimes and intensities are summarized as follows:

- The RCM12 simulation produces a similar number and duration of ETCs as ERA5, with a peak activity in the fall. Given that RCM12 is directly driven by ERA5 and employs spectral nudging in the interior of the domain, the close agreement between the two is expected. The RCM2.5 simulation evolves more freely (no interior nudging is used) and simulates a higher number of storms compared to both ERA5 and RCM12, indicating a peak activity in winter.
- The RCM2.5 simulation shows storms that are more frequent and longer-lasting than ERA5, especially in summer. It remains unclear whether this reflects an error or a more accurate representation of cyclone behaviour.
- Storm intensity, assessed via the 200-km radius averaged 850-hPa vorticity around cyclone's centers, is well simulated in both simulations, with the highest values in winter (DJF) and lowest in summer (JJA). This agreement may partly reflect the effect of spatial smoothing, as vorticity fields were smoothed with a 400-km Cressman filter before running the storm tracking algorithm and subsequently averaged over a 200-km radius around ETC centers.

The main findings regarding the ETC-associated surface wind speeds and precipitation are as follows :

- When compared with datasets of similar resolution to account for spatial representativity, both model versions reproduce the main features of the precipitation intensity-frequency distributions relatively well, with the most extreme rates captured during JJA. The RCM12 simulation underestimates extremes compared to radar and in situ data but agrees well with IMERG. Similarly, despite RCM2.5 tending to overestimate high precipitation rates, the simulation aligns closely with the higher-resolution StageIV dataset.
- Both simulations reasonably capture the seasonal cycle of ETC-associated surface winds, with stronger winds generally occurring in DJF, MAM and SON. The RCM12 overestimates near-surface wind speeds, while RCM2.5 reduces the discrepancy relative to ISD2ERA observations.

Overall, while both simulations perform well given their resolutions, the findings in this study suggest that the convection-permitting RCM2.5 is better suited for localized impact studies. Consistent with previous CPRCM assessments conducted over Europe (Leutwyler et al., 2016; Schaaf & Feser, 2018), these findings suggest that the added value of convection-permitting modeling in reproducing ETC-related surface fields is a robust characteristic across midlatitude regions.

The results of this study provide insight into the effects of dynamical downscaling on the simulation ETCs and their associated surface fields over northeastern North America. Although a higher frequency of ETC events often corresponds to greater ETC-associated precipitation totals, this relationship is not monotonic. To clarify the drivers behind the increased number of longer-lasting simulated storms and the more frequent occurrence of high precipitation rates during ETC events, future work should investigate the role of latent heat processes in ETCs at convection-permitting scales and their feedback on storm duration. One possible approach would be to compare multiple model configurations with parameterized and explicitly resolved deep convection and assess whether simulations producing stronger precipitation rates also yield longer-lived ETCs as a result of latent heating feedbacks. Finally, focused analyses on the most intense cyclones, in terms of surface winds and extreme precipitation, would be valuable. Creating climatologies specific to these events would help assess the model's skill in reproducing them and explore the potential impacts of climate change on their frequency and intensity.

CONCLUSION

Cette étude évalue la performance du modèle CRCM6-GEM5 pour la simulation des ETCs et leurs champs de surface associés au nord-est de l'Amérique du Nord de 2012 à 2022. Deux simulations possédant différentes grilles horizontales ont été analysées :

1. RCM12 : une version à 12 km de résolution horizontale, utilisant un schéma de paramétrage de la convection profonde et pilotée par la réanalyse ERA5 ;
2. RCM2.5 : une version à 2,5 km de résolution horizontale, avec représentation explicite de la convection profonde et pilotée par RCM12.

Les trajectoires simulées des tempêtes, ainsi que leur intensité et leur durée de vie, ont été comparées aux produits d'ERA5. Les champs de précipitation et de vents près de la surface associés aux ETCs ont été évalués à partir d'ERA5 et de diverses sources d'observation, incluant le jeu de données satellitaires IMERG, les données radar StageIV et les observations in situ issues du réseau ISD.

Les principaux résultats sur les trajectoires et caractéristiques des ETCs sont les suivants :

- La simulation RCM12 reproduit un nombre et une durée de vie d'ETCs similaires à ERA5, avec un maximum d'activité en automne, ce qui était attendu compte tenu du pilotage par la réanalyse et la contrainte spectrale appliquée au forçage à l'intérieur du domaine. En revanche, RCM2.5, qui n'emploie pas de contrainte spectrale, simule un plus grand nombre de tempêtes et ces dernières sont plus fréquentes l'hiver.
- La version à 2,5 km du modèle produit des tempêtes plus durables qu'ERA5, surtout en été. Ce biais pourrait découler d'un relâchement de chaleur latente plus intense, contribuant à une intensification accrue des systèmes. Il demeure incertain si ces écarts traduisent de véritables biais du modèle ou, au contraire, une représentation plus fidèle du comportement réel des cyclones.
- L'intensité, mesurée par le tourbillon à 850 hPa, est correctement représentée dans les deux configurations, avec un maximum en hiver et un minimum en été. Toutefois, cet accord pourrait être influencé par le lissage spatial appliqué aux champs de tourbillon avant l'algorithme de suivi.

Les principaux résultats sur les champs de précipitation et de vent près de la surface associés aux ETCs sont les suivantes :

- Lorsque comparées à des produits de référence possédant des résolutions horizontales similaires, les deux simulations reproduisent de manière satisfaisante les distributions intensité-fréquence de la précipitation, capturant les taux extrêmes en été. La simulation RCM12 sous-estime les précipitations extrêmes par rapport aux observations radar et in situ, mais correspond bien aux données IMERG. RCM2.5 surestime ces taux extrêmes, mais tout en restant proche des observations StageIV.
- Les deux versions reproduisent correctement la saisonnalité des vents près de la surface, avec un maximum en hiver, suivi du printemps et de l'automne. RCM12 tend à surestimer les vitesses, tandis que RCM2.5 réduit cet écart par rapport aux observations in situ.

En somme, les deux simulations performent raisonnablement bien en tenant compte des limites de leurs résolutions horizontales, mais les résultats suggèrent que la simulation permettant la convection explicite est plus appropriée pour des études climatiques locales. Certaines limites doivent toutefois être soulignées. D'abord, bien que le domaine de la simulation RCM2.5 ait été élargi afin de couvrir l'ensemble de l'Amérique du Nord en combinant les champs de pression et de tourbillon à 850 hPa avec ceux de RCM12 et d'ERA5, les sorties à 2,5 km demeurent disponibles sur une région restreinte et pour une période relativement courte (2012-2022). Un domaine plus étendu pourrait permettre à la haute résolution de mieux représenter, par exemple, le développement de cyclones additionnels et une série temporelle plus longue pourrait permettre de dégager des tendances climatiques plus robustes. Par ailleurs, l'évaluation des précipitations et des vents de surface a nécessité de réduire encore ce domaine à 195 points de grille situés dans le nord-est des États-Unis, limitant le nombre d'événements considérés. L'intégration de produits de référence complémentaires, tels que des réanalyses combinées à des observations satellitaires, permettrait d'inclure un plus grand nombre de points de grille et d'étendre l'analyse au Canada.

Ces limitations soulignent l'importance de poursuivre les investigations afin de mieux comprendre les mécanismes à l'origine des ETCs plus durables et des précipitations extrêmes plus fréquentes lorsque la convection profonde est résolue explicitement dans le modèle. Toutefois, bien que la fréquence plus élevée de trajectoires soit parfois associée à une augmentation des précipitations liées aux ETCs, cette relation n'est pas systématique. Pour mieux comprendre les mécanismes à l'origine de ce phénomène,

des travaux futurs devraient explorer le rôle des processus diabatiques liés au relâchement de chaleur latente. Une piste intéressante consisterait à comparer plusieurs configurations de modèles climatiques, avec et sans représentation explicite de la convection profonde, afin de déterminer si les précipitations les plus extrêmes sont associées à des ETCs plus durables en réponse à ces processus. Enfin, il serait pertinent de réaliser des analyses ciblées sur les cyclones les plus intenses en termes de vents de surface et de précipitations extrêmes. L'établissement de climatologies propres à ces événements permettrait d'évaluer la capacité du modèle à les reproduire et éventuellement, analyser l'influence potentielle des changements climatiques sur leur occurrence et leur intensité.

ANNEXE A

FIGURE SUPPLÉMENTAIRE : SAISONNALITÉ DE LA DURÉE DES ETCs

Cette annexe présente une figure supplémentaire permettant de compléter l'analyse portant sur la durée de vie des ETCs dans la section 1.4.1.2. Nous y retrouvons la distribution de l'occurrence de la durée de vie des ETCs dans le nord-est de l'Amérique du Nord, séparée entre les quatre saisons de l'année (Figure A.1).

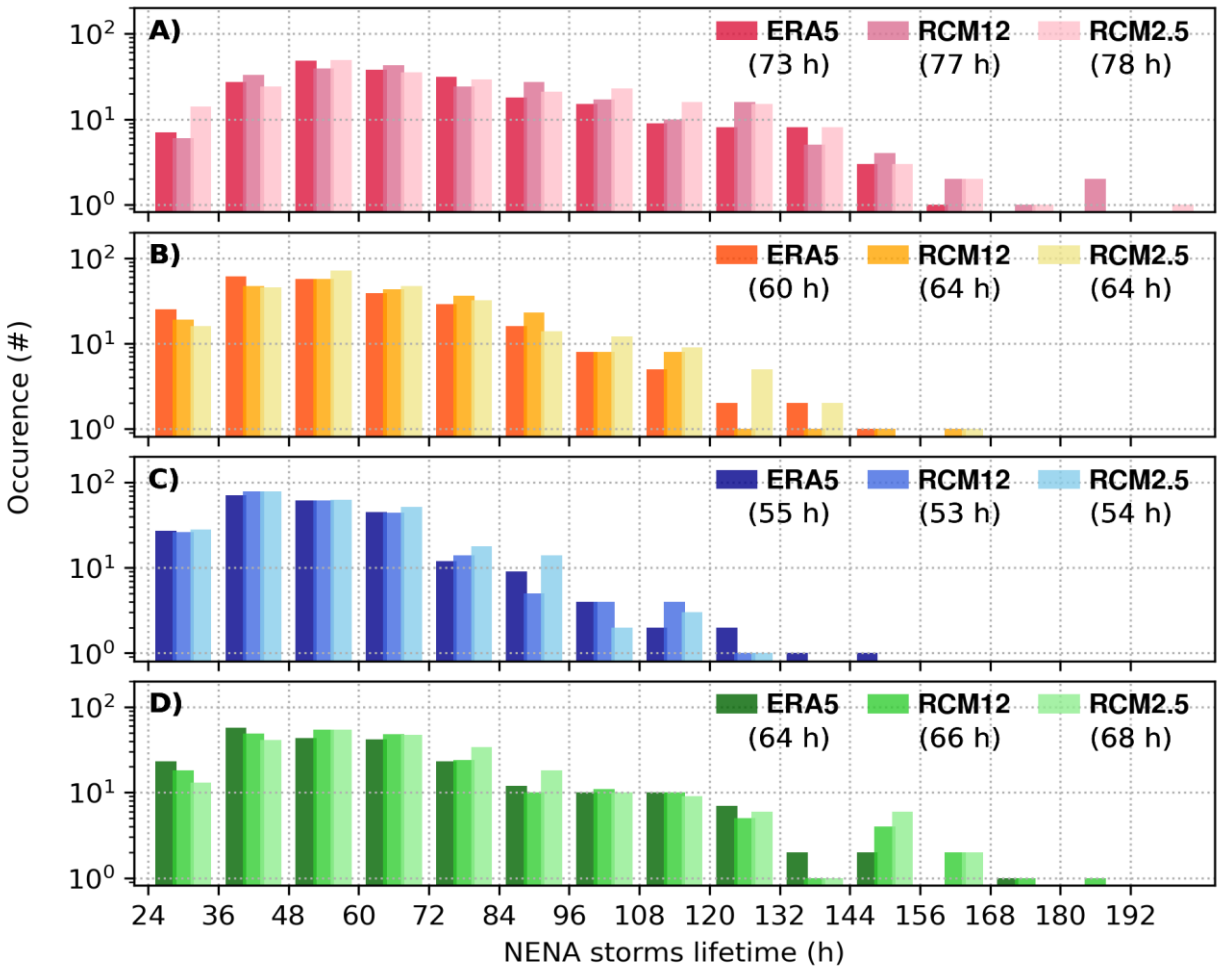

Figure A.1 : Distribution saisonnière de la durée de vie des cyclones extratropicaux dans le nord-est de l'Amérique du Nord (NENA) pour ERA5, RCM12 et RCM2.5, pour l'été (JJA; A), l'automne (SON; B), l'hiver (DJF; C) et le printemps (MAM; D). Les valeurs moyennes de chaque distribution pour chaque jeu de données sont indiquées dans le quadrant supérieur droit.

ANNEXE B

FIGURE SUPPLÉMENTAIRE : DISTRIBUTION DE L'OCCURENCE DES FAIBLES TAUX DE PRÉCIPITATION

Cette annexe présente une figure supplémentaire permettant de compléter l'analyse portant sur la fréquence des taux de précipitation associée aux ETCs dans la section 1.4.2.1. Nous y retrouvons la Figure B.1 qui présente la distribution de l'occurrence des taux de précipitation inférieurs ou égaux à 1 mm h^{-1} associés aux ETCs.

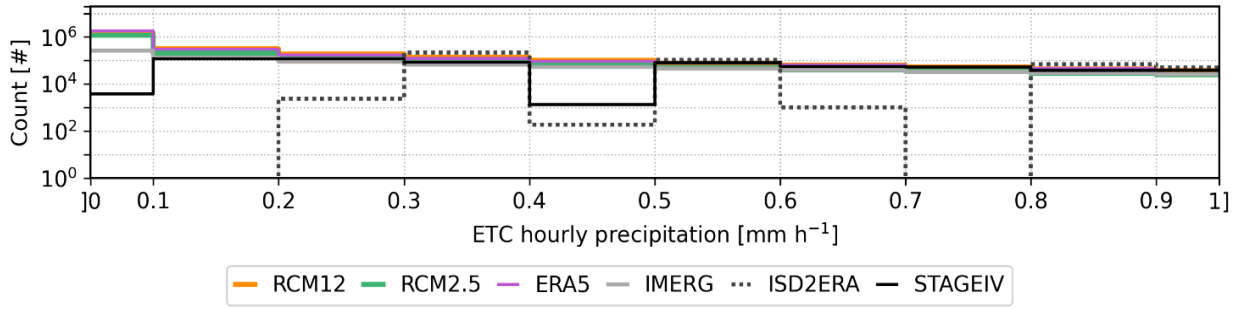

Figure B.1 : Distribution saisonnière du nombre d'occurrences de précipitations horaires associées aux ETCs, pour de faibles intensités (≤ 1 mm h^{-1}), toutes saisons confondues, pour les simulations RCM12 (orange) et RCM2.5 (vert), la réanalyse ERA5 (mauve) et les données d'observations de IMERG (gris), StageIV (ligne noire pleine) et ISD2ERA (ligne noire pointillée).

ANNEXE C

FIGURE SUPPLÉMENTAIRE : SAISONNALITÉ DES CHAMPS PRÈS DE LA SURFACE ASSOCIÉS AUX ETCs

La Figure C.1 présente la distribution saisonnière de l'occurrence des événements de précipitation horaire associés aux ETCs dépassant 15 mm h^{-1} (Figure C.1a) ainsi que des vitesses de vent près de la surface supérieures à 16 m s^{-1} (Figure C.1b), calculées sur les 195 points de grille d'analyse au nord-est des États-Unis. Ces seuils ont été sélectionnés à partir des figures 1.6 et 1.7, car ils correspondent aux valeurs à partir desquelles le taux horaire de précipitation et la vitesse du vent sont élevés, tout en contenant un nombre raisonnable de valeurs pour chaque jeu de données (une centaine environ).

Les principaux constats présentés à la section 1.4.2 concernant les taux extrêmes de précipitation et les vents forts se retrouvent clairement dans cette figure, notamment la sous-estimation systématique d'ERA5 pour les extrêmes de vent et de précipitation, ainsi que la divergence marquée de la distribution saisonnière d'IMERG par rapport aux autres produits. La Figure C.1a illustre la surestimation du taux de précipitation par la version à 2.5 km du modèle (RCM2.5), alors que la version à 12 km (RCM12) reproduit moins bien les taux extrêmes observés par les radars et stations in situ. La Figure C.1b montre la surestimation des vitesses de vent par RCM12, et l'atténuation de ce biais avec RCM2.5. Enfin, cette figure souligne le contraste marqué entre les distributions saisonnières des précipitations extrêmes et du vent. L'été correspond à des événements d'ETCs marqués par des précipitations maximales, mais à des vitesses de vent minimales, tandis que l'hiver présente les vents les plus forts, accompagnés de précipitations plus faibles.

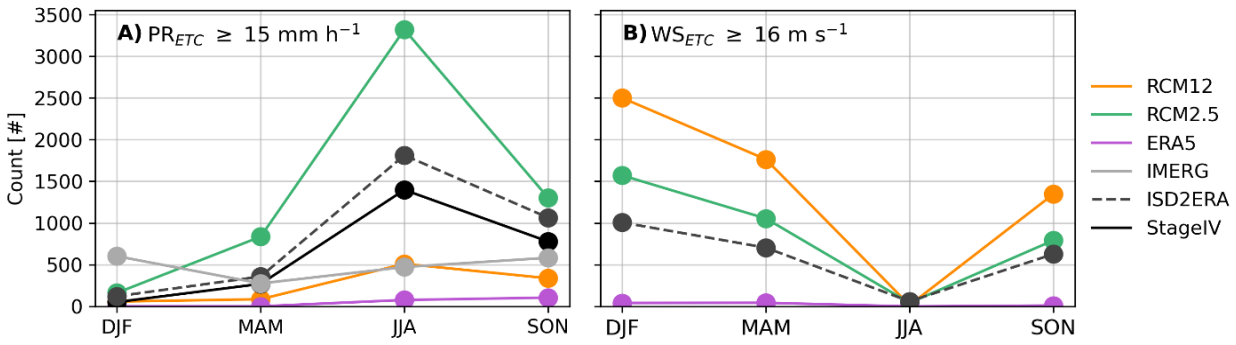

Figure C.1 : Distribution saisonnière de l'occurrence (A) des précipitations horaires associées aux ETCs ($PR_{ETC} \geq 16$ mm h^{-1}) et (B) des vitesses de vent près de la surface ($WS_{ETC} \geq 16$ m s^{-1}) pour les simulations RCM12 (orange) et RCM2.5 (vert), la réanalyse ERA5 (mauve) et les données d'observations de IMERG (gris), StageIV (ligne noire pleine) et ISD2ERA (ligne noire pointillée).

ANNEXE D

FIGURES SUPPLÉMENTAIRES : SENSIBILITÉ AU CHOIX DE SEUIL DU TAUX DE PRÉCIPITATION

La figure D.1 présente la décomposition des biais de précipitations associées aux ETC en utilisant un seuil de θ = 0.2 mm h^{-1}, mettant en évidence la sensibilité des résultats au choix du seuil pour les faibles taux de précipitation. Alors que les résultats pour RCM2.5 restent similaires entre un seuil de 1 mm h^{-1} (Figure 1.7q-ff) et 0,2 mm h^{-1} (Figure D.1q–ff), la simulation RCM12 montre une différence notable. Plutôt que de sous-estimer les précipitations totales associées aux ETC par rapport à StageIV et IMERG au seuil de 1 mm h^{-1} (Figure 1.7e,i), la décomposition avec le seuil plus bas révèle une surestimation prédominante des taux de précipitation par le modèle (Figure D.1e,i).

Les figures Figure D.2 et Figure D.3 présentent les précipitations totales normalisées associées aux ETC en utilisant des seuils respectifs de 0,2 mm h^{-1} et 1 mm h^{-1}. Abaisser le seuil augmente la précipitation totale normalisée associée aux ETC pour RCM12 d'environ 0,054 mm h^{-1} (Figure D.2a) à 0,074 mm h^{-1} (Figure D.3a), soit une augmentation de 0,02 mm h^{-1}. En comparaison, RCM2.5 et les jeux de données observationnels montrent une augmentation plus faible d'environ 0,01 mm h^{-1}. Cela suggère que RCM12 produit plus fréquemment des précipitations de faible intensité (< 0,2 mm h^{-1}) que les autres jeux de données. La réduction du seuil augmente la précipitation totale et réduit l'importance des biais négatifs. ERA5 présente également une augmentation d'environ 0,02 mm h^{-1} (Figure D.2c et Figure D.3c), ce qui peut expliquer pourquoi le biais de RCM12 par rapport à ERA5 reste similaire pour les deux seuils (Figure D.3a et Figure 1.7a).

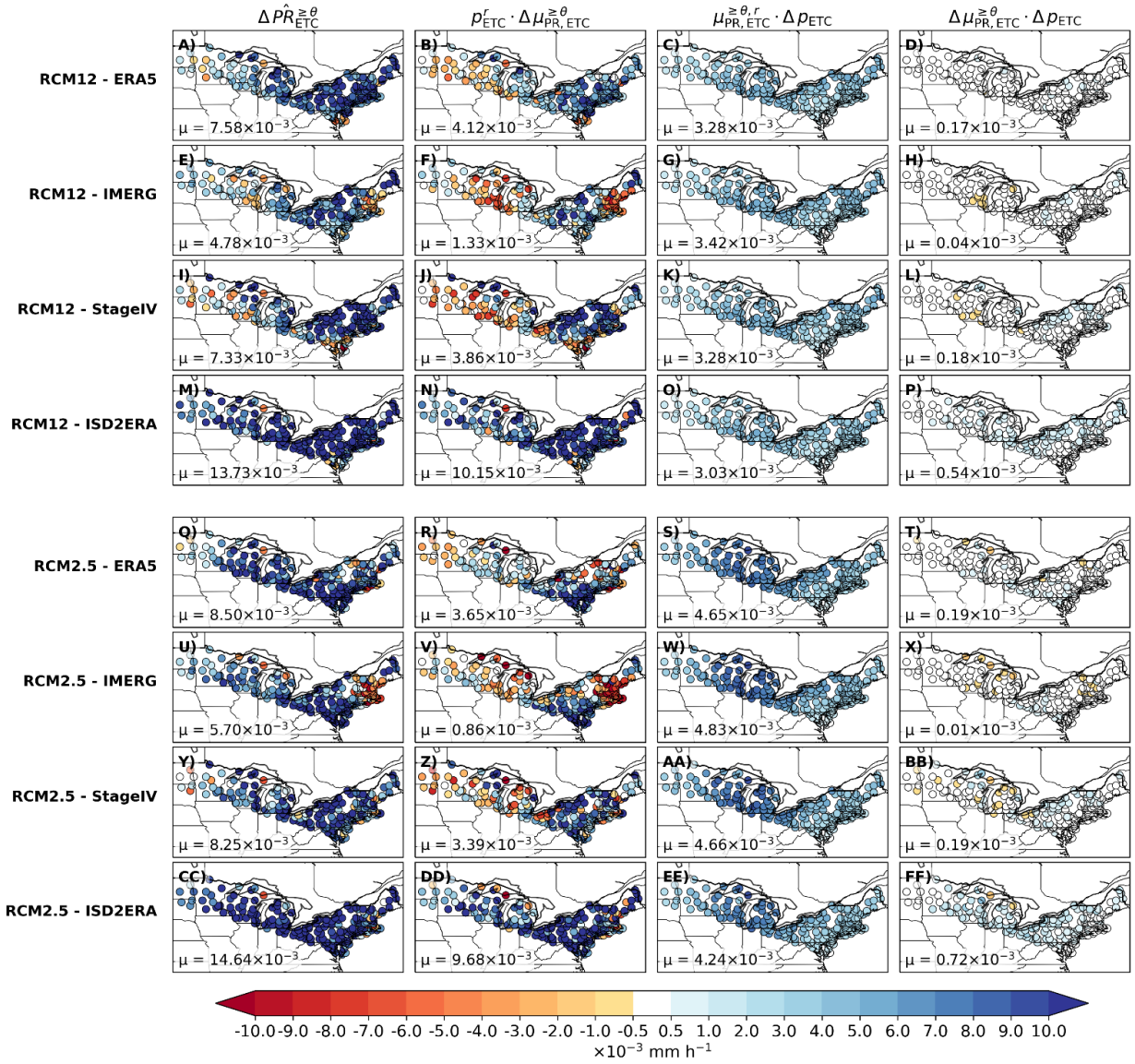

Figure D.1 : Décomposition du biais de la précipitation horaire normalisée associée aux ETCs (θ = 0.2 mm h^{-1}) pour RCM12 comparé à ERA5 (A-D), IMERG (E-H), StageIV (I-L) et ISD2ERA (M-P), ainsi que pour RCM2.5 comparé à ERA5 (Q-T), IMERG (U-V), StageIV (Y-BB) et ISD2ERA (CC-FF). Chaque colonne correspond à un terme de l'équation 6 : les colonnes A-CC montrent le biais total, les colonnes B-DD, le biais d'intensité des précipitations, les colonnes C-EE, le biais de trajectoire, et les colonnes D-FF, le biais d'interaction. Les nombres indiqués dans le coin inférieur gauche de chaque graphique représentent la valeur moyenne sur l'ensemble des stations.

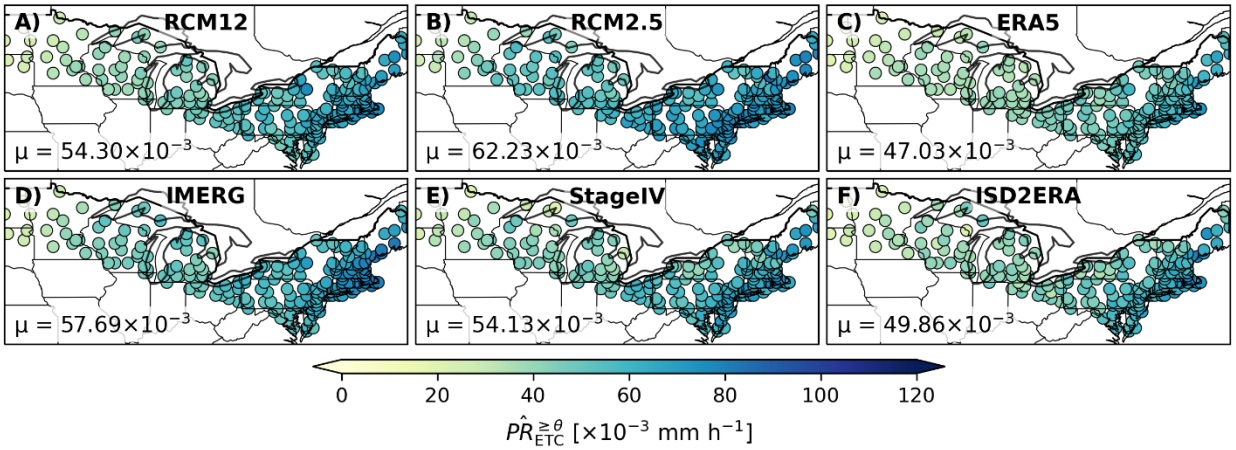

Figure D.2 : Précipitations totales normalisées associées aux ETCs (telles que décrites à la Section 1.3.3.1) pour les ensembles de données RCM12 (A), RCM2.5 (B), ERA5 (C), IMERG (D), StageIV (E) et ISD2ERA (F) en utilisant un seuil de θ = 1 mm h^{-1}. Les chiffres indiqués dans le coin inférieur gauche de chaque graphique représentent la valeur moyenne sur l'ensemble des stations.

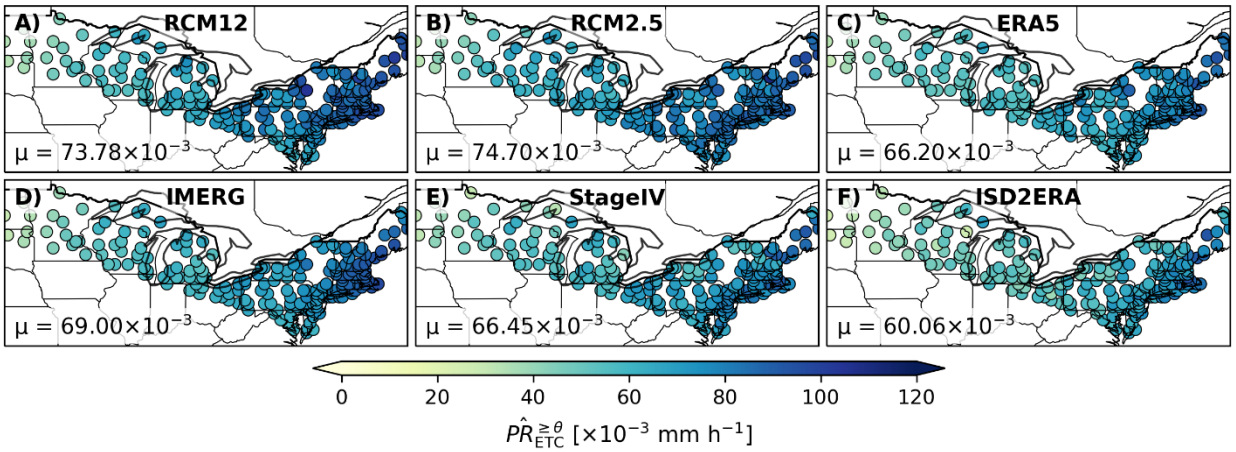

Figure D.3 : Identique à la Figure D.2, mais avec un seuil de 0.2 mm h^{-1}.

ANNEXE E

FIGURES SUPPLÉMENTAIRES : VITESSE NORMALISÉE DU VENT PRÈS DE LA SURFACE ASSOCIÉE AUX ETCs

Cette annexe présente une figure supplémentaire permettant de compléter l'analyse portant sur la décomposition des erreurs des champs près de la surface associés aux ETCs (section 1.4.1.2). Nous y retrouvons la qui présente les champs normalisés de la vitesse du vent près de la surface associés à des épisodes d'ETCs pour les deux simulations du modèle, la réanalyse ERA5 et les observations des stations ISD2ERA.

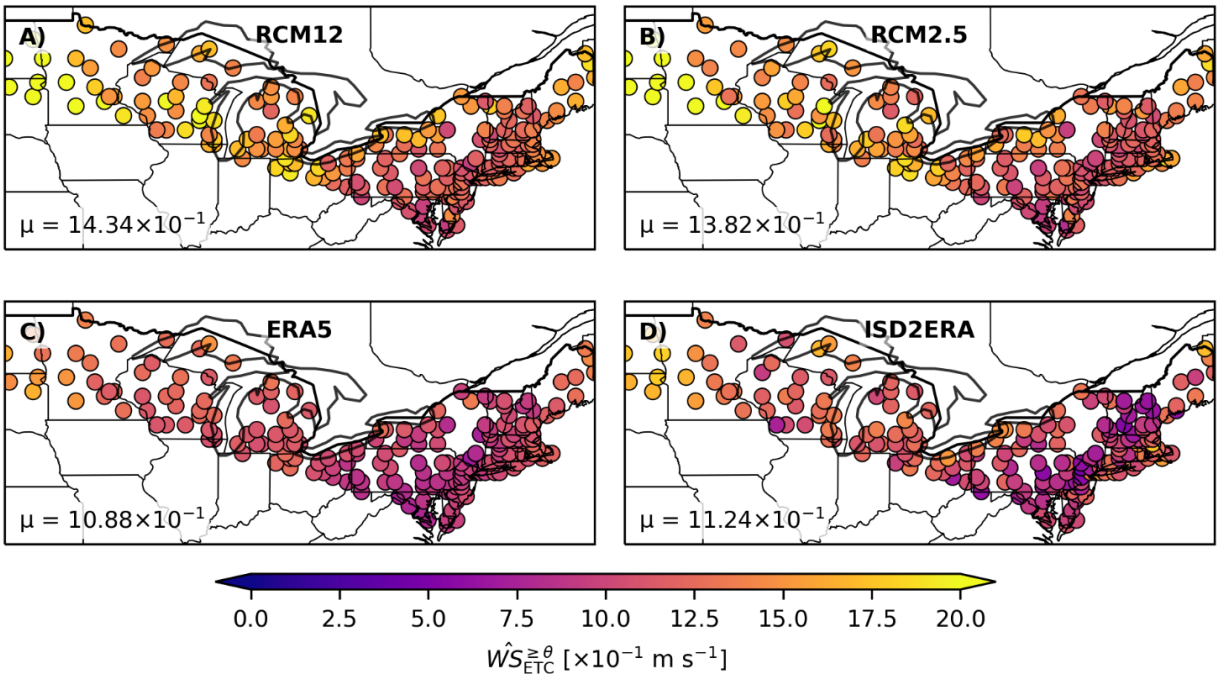

Figure E.1 : Champs de la vitesse du vent près de la surface normalisés associés aux ETCs (telles que décrites à la Section 1.3.3.1) pour les ensembles de données RCM12 (A), RCM2.5 (B), ERA5 (C) et ISD2ERA (D) en utilisant un seuil de $\theta = 0$ m s^{-1}. Les chiffres indiqués dans le coin inférieur gauche de chaque graphique représentent la valeur moyenne sur l'ensemble des stations.

RÉFÉRENCES

Ashley, W. S., & Black, A. W. (2008). Fatalities Associated with Nonconvective High-Wind Events in the United States. *Journal of Applied Meteorology and Climatology*, *47*(2), 717-725. https://doi.org/https://doi.org/10.1175/2007JAMC1689.1

Ban, N., Caillaud, C., Coppola, E., Pichelli, E., Sobolowski, S., Adinolfi, M., Ahrens, B., Alias, A., Anders, I., Bastin, S., Belušić, D., Berthou, S., Brisson, E., Cardoso, R. M., Chan, S. C., Christensen, O. B., Fernández, J., Fita, L., Frisius, T.,…Zander, M. J. (2021). The first multi-model ensemble of regional climate simulations at kilometer-scale resolution, part I: evaluation of precipitation. *Climate Dynamics*, *57*(1), 275-302. https://doi.org/10.1007/s00382-021-05708-w

Ban, N., Schmidli, J., & Schär, C. (2014). Evaluation of the convection-resolving regional climate modeling approach in decade-long simulations. *Journal of Geophysical Research: Atmospheres*, *119*(13), 7889-7907. https://doi.org/https://doi.org/10.1002/2014JD021478

Bechtold, P., Bazile, E., Guichard, F., Mascart, P., & Richard, E. (2001). A mass-flux convection scheme for regional and global models. *Quarterly Journal of the Royal Meteorological Society*, *127*(573), 869-886. https://doi.org/https://doi.org/10.1002/qj.49712757309

Belušić, A., Prtenjak, M. T., Güttler, I., Ban, N., Leutwyler, D., & Schär, C. (2018). Near-surface wind variability over the broader Adriatic region: insights from an ensemble of regional climate models. *Climate Dynamics*, *50*(11), 4455-4480. https://doi.org/10.1007/s00382-017-3885-5

Belušić Vozila, A., Belušić, D., Telišman Prtenjak, M., Güttler, I., Bastin, S., Brisson, E., Demory, M.-E., Dobler, A., Feldmann, H., & Hodnebrog, Ø. (2024). Evaluation of the near-surface wind field over the Adriatic region: local wind characteristics in the convection-permitting model ensemble. *Climate Dynamics*, *62*(6), 4617-4634.

Berthou, S., Kendon, E. J., Chan, S. C., Ban, N., Leutwyler, D., Schär, C., & Fosser, G. (2020). Pan-European climate at convection-permitting scale: a model intercomparison study. *Climate Dynamics*, *55*(1), 35-59. https://doi.org/10.1007/s00382-018-4114-6

Boisvert, L., Grecu, M., & Shie, C.-L. (2021). Investigating Wintertime GPM-IMERG Precipitation in the North Atlantic. *Geophysical Research Letters*, *48*(20), e2021GL095391. https://doi.org/https://doi.org/10.1029/2021GL095391

Booth, J. F., Naud, C. M., & Willison, J. (2018). Evaluation of Extratropical Cyclone Precipitation in the North Atlantic Basin: An Analysis of ERA-Interim, WRF, and Two CMIP5 Models. *Journal of Climate*, *31*(6), 2345-2360. https://doi.org/https://doi.org/10.1175/JCLI-D-17-0308.1

Booth, J. F., Rieder, H. E., Lee, D. E., & Kushnir, Y. (2015). The Paths of Extratropical Cyclones Associated with Wintertime High-Wind Events in the Northeastern United States. *Journal of Applied*

Meteorology and Climatology, *54*(9), 1871-1885. https://doi.org/https://doi.org/10.1175/JAMC-D-14-0320.1

Bozkurt, D., Bromwich, D. H., Carrasco, J., & Rondanelli, R. (2021). Temperature and precipitation projections for the Antarctic Peninsula over the next two decades: contrasting global and regional climate model simulations. *Climate Dynamics*, *56*(11), 3853-3874. https://doi.org/10.1007/s00382-021-05667-2

Catto, J. L., Ackerley, D., Booth, J. F., Champion, A. J., Colle, B. A., Pfahl, S., Pinto, J. G., Quinting, J. F., & Seiler, C. (2019). The Future of Midlatitude Cyclones. *Current Climate Change Reports*, *5*(4), 407-420. https://doi.org/10.1007/s40641-019-00149-4

Chan, S. C., Kendon, E. J., Berthou, S., Fosser, G., Lewis, E., & Fowler, H. J. (2020). Europe-wide precipitation projections at convection permitting scale with the Unified Model. *Climate Dynamics*, *55*(3), 409-428. https://doi.org/10.1007/s00382-020-05192-8

Chan, S. C., Kendon, E. J., Fowler, H. J., Blenkinsop, S., Ferro, C. A. T., & Stephenson, D. B. (2013). Does increasing the spatial resolution of a regional climate model improve the simulated daily precipitation? *Climate Dynamics*, *41*(5), 1475-1495. https://doi.org/10.1007/s00382-012-1568-9

Chang, W., Wang, J., Marohnic, J., Kotamarthi, V. R., & Moyer, E. J. (2020). Diagnosing added value of convection-permitting regional models using precipitation event identification and tracking. *Climate Dynamics*, *55*(1), 175-192. https://doi.org/10.1007/s00382-018-4294-0

Chartrand, J., & Pausata, F. S. R. (2020). Impacts of the North Atlantic Oscillation on winter precipitations and storm track variability in southeast Canada and the northeast United States. *Weather Clim. Dynam.*, *1*(2), 731-744. https://doi.org/10.5194/wcd-1-731-2020

Chen, C.-T., & Knutson, T. (2008). On the Verification and Comparison of Extreme Rainfall Indices from Climate Models. *Journal of Climate*, *21*(7), 1605-1621. https://doi.org/https://doi.org/10.1175/2007JCLI1494.1

Chen, T.-C., Collet, F., & Di Luca, A. (2024). Evaluation of ERA5 precipitation and 10-m wind speed associated with extratropical cyclones using station data over North America. *International Journal of Climatology*, *44*(3), 729-747. https://doi.org/10.1002/joc.8339

Chen, T.-C., Di Luca, A., Winger, K., Laprise, R., & Thériault, J. M. (2022). Seasonality of Continental Extratropical-Cyclone Wind Speeds Over Northeastern North America. *Geophysical Research Letters*, *49*(15). https://doi.org/https://doi.org/10.1029/2022GL098776

Chen, T. C., & Di Luca, A. (2025). Characteristics of precipitation and wind extremes induced by extratropical cyclones in northeastern North America. *Journal of Geophysical Research: Atmospheres*, *130*(6), e2024JD042079.

Cholette, M., Laprise, R., & Thériault, J. M. (2015). Perspectives for Very High-Resolution Climate Simulations with Nested Models: Illustration of Potential in Simulating St. Lawrence River Valley Channelling Winds with the Fifth-Generation Canadian Regional Climate Model. *Climate*, *3*(2), 283-307. https://www.mdpi.com/2225-1154/3/2/283

Chosson, F., Vaillancourt, P. A., Milbrandt, J. A., Yau, M. K., & Zadra, A. (2014). Adapting Two-Moment Microphysics Schemes across Model Resolutions: Subgrid Cloud and Precipitation Fraction and Microphysical Sub–Time Step. *Journal of the Atmospheric Sciences*, *71*(7), 2635-2653. https://doi.org/https://doi.org/10.1175/JAS-D-13-0367.1

Colle, B. A., Booth, J. F., & Chang, E. K. M. (2015). A Review of Historical and Future Changes of Extratropical Cyclones and Associated Impacts Along the US East Coast. *Current Climate Change Reports*, *1*(3), 125-143. https://doi.org/10.1007/s40641-015-0013-7

Colle, B. A., Zhang, Z., Lombardo, K. A., Chang, E., Liu, P., & Zhang, M. (2013). Historical Evaluation and Future Prediction of Eastern North American and Western Atlantic Extratropical Cyclones in the CMIP5 Models during the Cool Season. *Journal of Climate*, *26*(18), 6882-6903. https://doi.org/https://doi.org/10.1175/JCLI-D-12-00498.1

Collet, F., Di Luca, A., & Chen, T.-C. (2022). *North America ISD to ERA5 (NA-ISD2ERA) Catalogue* (Version V2) Borealis. https://doi.org/doi:10.5683/SP3/LWMGRM

Coppola, E., Giorgi, F., Giuliani, G., Pichelli, E., Ciarlo, J. M., Raffaele, F., Nogherotto, R., Reboita, M. S., Lu, C., & Zazulie, N. (2024). The Fifth Generation Regional Climate Modeling System, RegCM5: the first CP European wide simulation and validation over the CORDEX-CORE domains. *Authorea Preprints*.

Côté, H., Grise, K. M., Son, S.-W., de Elía, R., & Frigon, A. (2015). Challenges of tracking extratropical cyclones in regional climate models. *Climate Dynamics*, *44*(11), 3101-3109. https://doi.org/10.1007/s00382-014-2327-x

Côté, J., Gravel, S., Méthot, A., Patoine, A., Roch, M., & Staniforth, A. (1998). The Operational CMC–MRB Global Environmental Multiscale (GEM) Model. Part I: Design Considerations and Formulation. *Monthly Weather Review*, *126*(6), 1373-1395. https://doi.org/https://doi.org/10.1175/1520-0493(1998)126<1373:TOCMGE>2.0.CO;2

Crawford, A. D., McCrystall, M. R., Lukovich, J. V., & Stroeve, J. C. (2023). The Response of Extratropical Cyclone Propagation in the Northern Hemisphere to Global Warming. *Journal of Climate*, *36*(20), 7123-7142. https://doi.org/https://doi.org/10.1175/JCLI-D-23-0082.1

Dai, A., Rasmussen, R. M., Liu, C., Ikeda, K., & Prein, A. F. (2020). A new mechanism for warm-season precipitation response to globalwarming based on convection-permitting simulations. *Climate Dynamics*, *55*(1), 343-368. https://doi.org/10.1007/s00382-017-3787-6

Di Luca, A., Argüeso, D., Sherwood, S., & Evans, J. P. (2021). Evaluating Precipitation Errors Using the Environmentally Conditioned Intensity-Frequency Decomposition Method. *Journal of Advances in Modeling Earth Systems*, *13*(7), e2020MS002447. https://doi.org/https://doi.org/10.1029/2020MS002447

Di Luca, A., Evans, J. P., Pepler, A. S., Alexander, L. V., & Argüeso, D. (2016). Evaluating the representation of Australian East Coast Lows in a regional climate model ensemble. *Journal of Southern Hemisphere Earth Systems Science*, *66*(2), 108-124. https://doi.org/10.1071/ES16011

ElBessa, M., Abdelrahman, S. M., Tonbol, K., & Shaltout, M. (2021). Dynamical Downscaling of Surface Air Temperature and Wind Field Variabilities over the Southeastern Levantine Basin, Mediterranean Sea. *Climate*, *9*(10), 150. https://www.mdpi.com/2225-1154/9/10/150

Evans, J. P., & McCabe, M. F. (2013). Effect of model resolution on a regional climate model simulation over southeast Australia. *Climate Research*, *56*, 131-145.

Fosser, G., Khodayar, S., & Berg, P. (2015). Benefit of convection permitting climate model simulations in the representation of convective precipitation. *Climate Dynamics*, *44*(1), 45-60. https://doi.org/10.1007/s00382-014-2242-1

Gilliland, J. M., Black, A. W., Durkee, J. D., & Murley, V. A. (2020). A climatology of high‐wind events for the eastern United States. *International Journal of Climatology*, *40*(2), 723-738.

Giorgi, F. (2019). Thirty Years of Regional Climate Modeling: Where Are We and Where Are We Going next? *Journal of Geophysical Research: Atmospheres*, *124*(11), 5696-5723. https://doi.org/https://doi.org/10.1029/2018JD030094

Giorgi, F., & Gutowski, W. J. (2015). Regional Dynamical Downscaling and the CORDEX Initiative. *Annual Review of Environment and Resources*, *40*(Volume 40, 2015), 467-490. https://doi.org/https://doi.org/10.1146/annurev-environ-102014-021217

Giorgi, F., Jones, C., & Asrar, G. (2006). Addressing climate information needs at the regional level: The CORDEX framework. *World Meteorological Organization Bulletin*, *58*(3), 175.

Gurgel, A. d. R. C., Sales, D. C., & Lima, K. C. (2024). Wind power density in areas of Northeastern Brazil from Regional Climate Models for a recent past. *PloS one*, *19*(7), e0307641.

Haarsma, R. J., Roberts, M. J., Vidale, P. L., Senior, C. A., Bellucci, A., Bao, Q., Chang, P., Corti, S., Fučkar, N. S., Guemas, V., von Hardenberg, J., Hazeleger, W., Kodama, C., Koenigk, T., Leung, L. R., Lu, J., Luo, J. J., Mao, J., Mizielinski, M. S.,…von Storch, J. S. (2016). High Resolution Model Intercomparison Project (HighResMIP v1.0) for CMIP6. *Geosci. Model Dev.*, *9*(11), 4185-4208. https://doi.org/10.5194/gmd-9-4185-2016

Hawcroft, M., Walsh, E., Hodges, K., & Zappa, G. (2018). Significantly increased extreme precipitation expected in Europe and North America from extratropical cyclones. *Environmental Research Letters*, *13*(12). https://doi.org/10.1088/1748-9326/aaed59

Hawcroft, M. K., Shaffrey, L. C., Hodges, K. I., & Dacre, H. F. (2012). How much Northern Hemisphere precipitation is associated with extratropical cyclones? *Geophysical Research Letters*, *39*(24). https://doi.org/https://doi.org/10.1029/2012GL053866

Hawcroft, M. K., Shaffrey, L. C., Hodges, K. I., & Dacre, H. F. (2016). Can climate models represent the precipitation associated with extratropical cyclones? *Climate Dynamics*, *47*(3), 679-695. https://doi.org/10.1007/s00382-015-2863-z

Hersbach, H., Bell, B., Berrisford, P., Hirahara, S., Horányi, A., Muñoz-Sabater, J., Nicolas, J., Peubey, C., Radu, R., Schepers, D., Simmons, A., Soci, C., Abdalla, S., Abellan, X., Balsamo, G., Bechtold, P., Biavati, G., Bidlot, J., Bonavita, M.,…Thépaut, J.-N. (2020). The ERA5 global reanalysis. *Quarterly Journal of the Royal Meteorological Society*, *146*(730), 1999-2049. https://doi.org/https://doi.org/10.1002/qj.3803

Hosseini-Moghari, S.-M., & Tang, Q. (2022). Can IMERG Data Capture the Scaling of Precipitation Extremes With Temperature at Different Time Scales? *Geophysical Research Letters*, *49*(3), e2021GL096392. https://doi.org/https://doi.org/10.1029/2021GL096392

Huffman, G. J., Bolvin, D. T., Braithwaite, D., Hsu, K.-L., Joyce, R. J., Kidd, C., Nelkin, E. J., Sorooshian, S., Stocker, E. F., & Tan, J. (2020). Integrated multi-satellite retrievals for the global precipitation measurement (GPM) mission (IMERG). *Satellite precipitation measurement: Volume 1*, 343-353.

Huffman, G. J., Bolvin, D. T., Joyce, R., Kelley, O. A., Nelkin, E. J., Portier, A., Stocker, E. F., Tan, J., Watters, D. C., & West, B. J. (2023). IMERG V07 Release Notes. In.

Insurance Bureau of Canada. (2019). *Halloween Storm Across Eastern Canada Caused Over $250 Million in Insured Damanges*. https://bac-quebec.qc.ca/en/insurance-issues/disaster/

Jiaxiang, G., Shoshiro, M., Roberts, M. J., Haarsma, R., Putrasahan, D., Roberts, C. D., Scoccimarro, E., Terray, L., Vannière, B., & Vidale, P. L. (2020). Influence of model resolution on bomb cyclones revealed by HighResMIP-PRIMAVERA simulations. *Environmental Research Letters*, *15*(8). https://doi.org/10.1088/1748-9326/ab88fa

Jones, C., Giorgi, F., & Asrar, G. (2011). The coordinated regional downscaling experiment (CORDEX). An international downscaling link to CMIP5. *CLIVAR exchanges*, *56*.

Jouan, C., Milbrandt, J. A., Vaillancourt, P. A., Chosson, F., & Morrison, H. (2020). Adaptation of the Predicted Particles Properties (P3) Microphysics Scheme for Large-Scale Numerical Weather Prediction. *Weather and Forecasting*, *35*(6), 2541-2565. https://doi.org/https://doi.org/10.1175/WAF-D-20-0111.1

Jung, T., Gulev, S. K., Rudeva, I., & Soloviov, V. (2006). Sensitivity of extratropical cyclone characteristics to horizontal resolution in the ECMWF model. *Quarterly Journal of the Royal Meteorological Society*, *132*(619), 1839-1857. https://doi.org/https://doi.org/10.1256/qj.05.212

Kain, J. S., & Fritsch, J. M. (1990). A One-Dimensional Entraining/Detraining Plume Model and Its Application in Convective Parameterization. *Journal of Atmospheric Sciences*, *47*(23), 2784-2802. https://doi.org/https://doi.org/10.1175/1520-0469(1990)047<2784:AODEPM>2.0.CO;2

Karypidou, M. C., Katragkou, E., & Sobolowski, S. P. (2022). Precipitation over southern Africa: is there consensus among global climate models (GCMs), regional climate models (RCMs) and observational data? *Geosci. Model Dev.*, *15*(8), 3387-3404. https://doi.org/10.5194/gmd-15-3387-2022

Kendon, E. J., Roberts, N. M., Senior, C. A., & Roberts, M. J. (2012). Realism of Rainfall in a Very High-Resolution Regional Climate Model. *Journal of Climate*, *25*(17), 5791-5806. https://doi.org/https://doi.org/10.1175/JCLI-D-11-00562.1

Lackmann, G. (2011). Midlatitude synoptic meteorology. *(No Title)*.

Lakku, N. K. G., & Behera, M. R. (2022). Skill and Inter-Model Comparison of Regional and Global Climate Models in Simulating Wind Speed over South Asian Domain. *Climate*, *10*(6), 85. https://www.mdpi.com/2225-1154/10/6/85

Laprise, R. (2008). Regional climate modelling. *Journal of computational physics*, *227*(7), 3641-3666.

Laprise, R., De Elia, R., Caya, D., Biner, S., Lucas-Picher, P., Diaconescu, E., Leduc, M., Alexandru, A., Separovic, L., Modelling, C. N. f. R. C., & Diagnostics. (2008). Challenging some tenets of regional climate modelling. *Meteorology and Atmospheric Physics*, *100*(1), 3-22.

Lee, M.-I., Schubert, S. D., Suarez, M. J., Held, I. M., Kumar, A., Bell, T. L., Schemm, J.-K. E., Lau, N.-C., Ploshay, J. J., Kim, H.-K., & Yoo, S.-H. (2007). Sensitivity to Horizontal Resolution in the AGCM Simulations of Warm Season Diurnal Cycle of Precipitation over the United States and Northern Mexico. *Journal of Climate*, *20*(9), 1862-1881. https://doi.org/https://doi.org/10.1175/JCLI4090.1

Letson, F. W., Barthelmie, R. J., Hodges, K. I., & Pryor, S. C. (2021). Intense windstorms in the northeastern United States. *Nat. Hazards Earth Syst. Sci.*, *21*(7), 2001-2020. https://doi.org/10.5194/nhess-21-2001-2021

Leutwyler, D., Fuhrer, O., Lapillonne, X., Lüthi, D., & Schär, C. (2016). Towards European-scale convection-resolving climate simulations with GPUs: a study with COSMO 4.19. *Geosci. Model Dev.*, *9*(9), 3393-3412. https://doi.org/10.5194/gmd-9-3393-2016

Li, M., Woollings, T., Hodges, K., & Masato, G. (2014). Extratropical cyclones in a warmer, moister climate: A recent Atlantic analogue. *Geophysical Research Letters*, *41*(23), 8594-8601. https://doi.org/https://doi.org/10.1002/2014GL062186

Lin, Y., & Mitchell, K. (2005). The NCEP stage II/IV hourly precipitation analyses: Development and applications.

Lipzig, N., Van de Walle, J., Belušić, D., Berthou, S., Coppola, E., Demuzere, M., Fink, A., Finney, D., Glazer, R., Ludwig, P., Marsham, J., Nikulin, G., Pinto, J., Rowell, D., Wu, M., & Thiery, W. (2022). Representation of precipitation and top-of-atmosphere radiation in a multi-model convection-permitting ensemble for the Lake Victoria Basin (East-Africa). *Climate Dynamics*, *60*, 1-22. https://doi.org/10.1007/s00382-022-06541-5

Lucas-Picher, P., Argüeso, D., Brisson, E., Tramblay, Y., Berg, P., Lemonsu, A., Kotlarski, S., & Caillaud, C. (2021). Convection-permitting modeling with regional climate models: Latest developments and next steps. *WIREs Climate Change*, *12*(6), e731. https://doi.org/https://doi.org/10.1002/wcc.731

Martynov, A., Laprise, R., Sushama, L., Winger, K., Šeparović, L., & Dugas, B. (2013). Reanalysis-driven climate simulation over CORDEX North America domain using the Canadian Regional Climate Model, version 5: model performance evaluation. *Climate Dynamics*, *41*(11), 2973-3005. https://doi.org/10.1007/s00382-013-1778-9

McTaggart-Cowan, R., Vaillancourt, P. A., Zadra, A., Chamberland, S., Charron, M., Corvec, S., Milbrandt, J. A., Paquin-Ricard, D., Patoine, A., Roch, M., Separovic, L., & Yang, J. (2019a). Modernization of Atmospheric Physics Parameterization in Canadian NWP. *Journal of Advances in Modeling Earth Systems*, *11*(11), 3593-3635. https://doi.org/https://doi.org/10.1029/2019MS001781

McTaggart-Cowan, R., Vaillancourt, P. A., Zadra, A., Separovic, L., Corvec, S., & Kirshbaum, D. (2019b). A Lagrangian Perspective on Parameterizing Deep Convection. *Monthly Weather Review*, *147*(11), 4127-4149. https://doi.org/https://doi.org/10.1175/MWR-D-19-0164.1

Milbrandt, J. A., & Morrison, H. (2016). Parameterization of Cloud Microphysics Based on the Prediction of Bulk Ice Particle Properties. Part III: Introduction of Multiple Free Categories. *Journal of the Atmospheric Sciences*, *73*(3), 975-995. https://doi.org/https://doi.org/10.1175/JAS-D-15-0204.1

Morrison, H., & Milbrandt, J. A. (2015). Parameterization of Cloud Microphysics Based on the Prediction of Bulk Ice Particle Properties. Part I: Scheme Description and Idealized Tests. *Journal of the Atmospheric Sciences*, *72*(1), 287-311. https://doi.org/https://doi.org/10.1175/JAS-D-14-0065.1

Morrison, H., Milbrandt, J. A., Bryan, G. H., Ikeda, K., Tessendorf, S. A., & Thompson, G. (2015). Parameterization of Cloud Microphysics Based on the Prediction of Bulk Ice Particle Properties. Part II: Case Study Comparisons with Observations and Other Schemes. *Journal of the Atmospheric Sciences*, *72*(1), 312-339. https://doi.org/https://doi.org/10.1175/JAS-D-14-0066.1

Nelson, B. R., Prat, O. P., & Leeper, R. D. (2021). An Investigation of NEXRAD-Based Quantitative Precipitation Estimates in Alaska. *Remote Sensing*, *13*(16), 3202. https://www.mdpi.com/2072-4292/13/16/3202

Nelson, B. R., Prat, O. P., Seo, D.-J., & Habib, E. (2016). Assessment and Implications of NCEP Stage IV Quantitative Precipitation Estimates for Product Intercomparisons. *Weather and Forecasting*, *31*(2), 371-394. https://doi.org/https://doi.org/10.1175/WAF-D-14-00112.1

Neu, U., Akperov, M. G., Bellenbaum, N., Benestad, R., Blender, R., Caballero, R., Cocozza, A., Dacre, H. F., Feng, Y., Fraedrich, K., Grieger, J., Gulev, S., Hanley, J., Hewson, T., Inatsu, M., Keay, K., Kew, S. F., Kindem, I., Leckebusch, G. C.,…Wernli, H. (2013). IMILAST: A Community Effort to Intercompare Extratropical Cyclone Detection and Tracking Algorithms. *Bulletin of the American Meteorological Society*, *94*(4), 529-547. https://doi.org/https://doi.org/10.1175/BAMS-D-11-00154.1

Pfahl, S., & Wernli, H. (2012). Quantifying the Relevance of Cyclones for Precipitation Extremes. *Journal of Climate*, *25*(19), 6770-6780. https://doi.org/https://doi.org/10.1175/JCLI-D-11-00705.1

Poan, E. D., Gachon, P., Laprise, R., Aider, R., & Dueymes, G. (2018). Investigating added value of regional climate modeling in North American winter storm track simulations. *Climate Dynamics*, *50*(5), 1799-1818. https://doi.org/10.1007/s00382-017-3723-9

Prat, O. P., & Nelson, B. R. (2015). Evaluation of precipitation estimates over CONUS derived from satellite, radar, and rain gauge data sets at daily to annual scales (2002–2012). *Hydrol. Earth Syst. Sci.*, *19*(4), 2037-2056. https://doi.org/10.5194/hess-19-2037-2015

Prein, A. F., Holland, G. J., Rasmussen, R. M., Done, J., Ikeda, K., Clark, M. P., & Liu, C. H. (2013). Importance of Regional Climate Model Grid Spacing for the Simulation of Heavy Precipitation in the Colorado Headwaters. *Journal of Climate*, *26*(13), 4848-4857. https://doi.org/https://doi.org/10.1175/JCLI-D-12-00727.1

Priestley, M. D. K., Ackerley, D., Catto, J. L., Hodges, K. I., McDonald, R. E., & Lee, R. W. (2020). An Overview of the Extratropical Storm Tracks in CMIP6 Historical Simulations. *Journal of Climate*, *33*(15), 6315-6343. https://doi.org/https://doi.org/10.1175/JCLI-D-19-0928.1

Priestley, M. D. K., & Catto, J. L. (2022). Future changes in the extratropical storm tracks and cyclone intensity, wind speed, and structure. *Weather Clim. Dynam.*, *3*(1), 337-360. https://doi.org/10.5194/wcd-3-337-2022

Roberge, F., Di Luca, A., Laprise, R., Lucas-Picher, P., & Thériault, J. (2024). Spatial spin-up of precipitation in limited-area convection-permitting simulations over North America using the CRCM6/GEM5.0 model. *Geosci. Model Dev.*, *17*(4), 1497-1510. https://doi.org/10.5194/gmd-17-1497-2024

Roberts, M. J., Reed, K. A., Bao, Q., Barsugli, J. J., Camargo, S. J., Caron, L. P., Chang, P., Chen, C. T., Christensen, H. M., Danabasoglu, G., Frenger, I., Fučkar, N. S., ul Hasson, S., Hewitt, H. T., Huang,

H., Kim, D., Kodama, C., Lai, M., Leung, L. Y. R.,…Zhao, M. (2025). High-Resolution Model Intercomparison Project phase 2 (HighResMIP2) towards CMIP7. *Geosci. Model Dev.*, *18*(4), 1307-1332. https://doi.org/10.5194/gmd-18-1307-2025

Rummukainen, M. (2016). Added value in regional climate modeling. *Wiley Interdisciplinary Reviews: Climate Change*, *7*(1), 145-159. https://doi.org/10.1002/wcc.378

Schaaf, B., & Feser, F. (2018). Is there added value of convection-permitting regional climate model simulations for storms over the German Bight and Northern Germany? *Meteorology Hydrology and Water Management. Research and Operational Applications*, *6*.

Seiler, C., & Zwiers, F. W. (2016). How well do CMIP5 climate models reproduce explosive cyclones in the extratropics of the Northern Hemisphere? *Climate Dynamics*, *46*(3), 1241-1256. https://doi.org/10.1007/s00382-015-2642-x

Seiler, C., Zwiers, F. W., Hodges, K. I., & Scinocca, J. F. (2018). How does dynamical downscaling affect model biases and future projections of explosive extratropical cyclones along North America's Atlantic coast? *Climate Dynamics*, *50*(1), 677-692. https://doi.org/10.1007/s00382-017-3634-9

Šeparović, L., Alexandru, A., Laprise, R., Martynov, A., Sushama, L., Winger, K., Tete, K., & Valin, M. (2013). Present climate and climate change over North America as simulated by the fifth-generation Canadian regional climate model. *Climate Dynamics*, *41*(11), 3167-3201. https://doi.org/10.1007/s00382-013-1737-5

Sibley, A. (2010). Analysis of extreme rainfall and flooding in Cumbria 18–20 November 2009. *Weather*, *65*(11), 287-292. https://doi.org/https://doi.org/10.1002/wea.672

Smalley, M., L'Ecuyer, T., Lebsock, M., & Haynes, J. (2014). A Comparison of Precipitation Occurrence from the NCEP Stage IV QPE Product and the CloudSat Cloud Profiling Radar. *Journal of Hydrometeorology*, *15*(1), 444-458. https://doi.org/https://doi.org/10.1175/JHM-D-13-048.1

Statistique Canada. (2025). *Horloge démographique du Canada (modèle en temps réel)* https://www150.statcan.gc.ca/n1/pub/71-607-x/71-607-x2018005-fra.htm

Tripathi, O. P., & Dominguez, F. (2013). Effects of spatial resolution in the simulation of daily and subdaily precipitation in the southwestern US. *Journal of Geophysical Research: Atmospheres*, *118*(14), 7591-7605. https://doi.org/https://doi.org/10.1002/jgrd.50590

Trzeciak, T. M., Knippertz, P., Pirret, J. S. R., & Williams, K. D. (2016). Can we trust climate models to realistically represent severe European windstorms? *Climate Dynamics*, *46*(11), 3431-3451. https://doi.org/10.1007/s00382-015-2777-9

United States Census Bureau. (2025). *U.S. and World Population Clock* https://www.census.gov/popclock/

Veilleux, K., Di Luca, A., Thériault, J. M., Poitras, V., Vaillancourt, P. A., Cholette, M., & Roberge, F. (2025). Assessing Cloud Fraction in the Canadian Regional Climate Model Over North America Using Satellite Data and a Satellite Simulator Package. *Journal of Geophysical Research: Atmospheres*, *130*(7), e2024JD042453. https://doi.org/https://doi.org/10.1029/2024JD042453

Wang, S., Qin, Y., Lu, C., & Guan, Z. (2023). An intensity index and its application for summertime extratropical cyclones in East Asia. *Geoscience Letters*, *10*(1), 13. https://doi.org/10.1186/s40562-023-00267-w

Whittaker, T., Di Luca, A., Roberge, F., & Winger, K. (2025). Evaluating Near-Surface Wind Speeds Simulated by the CRCM6-GEM5 Model Using AmeriFlux Data Over North America. *Journal of Advances in Modeling Earth Systems*, *17*(3), e2024MS004666. https://doi.org/https://doi.org/10.1029/2024MS004666

Willison, J., Robinson, W. A., & Lackmann, G. M. (2013). The Importance of Resolving Mesoscale Latent Heating in the North Atlantic Storm Track. *Journal of the Atmospheric Sciences*, *70*(7), 2234-2250. https://doi.org/https://doi.org/10.1175/JAS-D-12-0226.1

Yanai, M., & Johnson, R. H. (1993). Impacts of Cumulus Convection on Thermodynamic Fields. In K. A. Emanuel & D. J. Raymond (Eds.), *The Representation of Cumulus Convection in Numerical Models* (pp. 39-62). American Meteorological Society. https://doi.org/10.1007/978-1-935704-13-3_4

Zappa, G., Hawcroft, M. K., Shaffrey, L., Black, E., & Brayshaw, D. J. (2015). Extratropical cyclones and the projected decline of winter Mediterranean precipitation in the CMIP5 models. *Climate Dynamics*, *45*(7), 1727-1738. https://doi.org/10.1007/s00382-014-2426-8

Zappa, G., Shaffrey, L. C., & Hodges, K. I. (2013). The Ability of CMIP5 Models to Simulate North Atlantic Extratropical Cyclones. *Journal of Climate*, *26*(15), 5379-5396. https://doi.org/https://doi.org/10.1175/JCLI-D-12-00501.1

Zappa, G., Shaffrey, L. C., Hodges, K. I., Sansom, P. G., & Stephenson, D. B. (2013). A multimodel assessment of future projections of North Atlantic and European extratropical cyclones in the CMIP5 climate models. *Journal of Climate*, *26*(16), 5846-5862.

Zhang, M., Perrie, W., & Long, Z. (2019). Sensitivity Study of North Atlantic Summer Cyclone Activity in Dynamical Downscaled Simulations. *Journal of Geophysical Research: Atmospheres*, *124*(14), 7599-7616. https://doi.org/https://doi.org/10.1029/2018JD029766

Zhang, Z., & Colle, B. A. (2018). Impact of Dynamically Downscaling Two CMIP5 Models on the Historical and Future Changes in Winter Extratropical Cyclones along the East Coast of North America. *Journal of Climate*, *31*(20), 8499-8525. https://doi.org/https://doi.org/10.1175/JCLI-D-18-0178.1

Zhao, B., Hudak, D., Rodriguez, P., Mekis, E., Brunet, D., Eckert, E., & Melo, S. (2023). Assessment of IMERG v06 Satellite Precipitation Products in the Canadian Great Lakes Region. *Journal of Hydrometeorology*, *24*(6), 1017-1037. https://doi.org/https://doi.org/10.1175/JHM-D-22-0214.1